January 2011

Determining The Fate Of Bone Marrow Mononuclear Cells In Tissue Engineered Vascular Grafts Using Mri

Jamie Keiko Nicole Harrington
Yale School of Medicine, jkeikoharrington@gmail.com

Determining the Fate of Bone Marrow Mononuclear Cells in Tissue Engineered Vascular Grafts using MRI

A Thesis Submitted to the

Yale University School of Medicine

in Partial Fulfillment of the Requirements for the

Degree of Doctor of Medicine

by

Jamie Keiko Nicole Harrington

2011

Abstract

The most widely used method of creating tissue engineered vascular grafts (TEVGs) for *in vivo* implantation consists of seeding autologous bone marrow cells (BMCs) onto biodegradable scaffolds. In this model of TEVG development it has traditionally been thought that stem cells and endothelial progenitor cells (EPCs) within the seeded bone marrow population gave rise to the cells of the neovessel. Recent work in our lab indicates that the seeded BMCs are not incorporated into the neovessel and are actually rapidly lost from the implanted scaffold. Here we show the feasibility of noninvasively monitoring this process by tracking ultrasmall superparamagnetic iron oxide (USPIO) labeled macrophages with MRI. Murine macrophages were labeled with USPIO through *in vitro* culture in media containing 2mg/ml of USPIO. The USPIO-labeled macrophages were seeded onto polyglycolic acid (PGA) scaffolds that were surgically implanted as inferior vena cava interposition grafts in SCID/bg mice. Images were then obtained using a 4.7T Bruker horizontal bore scanner with an optimized RARE spin echo sequence and a multislice-multiecho sequence to determine the T2 relaxation time with serial imaging. The T2 signal was found to be significantly lower immediately following implantation of the USPIO labeled scaffolds (T2 = 44±6.8 vs. 71±10.2), but increased rapidly to a value identical to that of control implants seeded with unlabeled macrophages (T2 = 63±12 vs. 63±14). This strongly indicates the rapid loss of seeded cells from the scaffolds, a finding verified using Prussian blue staining for iron containing macrophages on histological sections of explanted TEVGs. Our findings provide further support for the paradigm shift away from BMC neovessel

incorporation towards the host cell based population of implanted TEVGs. Furthermore, we demonstrate one of the first successful applications of noninvasive MR imaging for serial study of cellular level processes in tissue engineering.

Acknowledgments

This work was performed in the lab of Christopher K. Breuer, M.D., in the Interdepartmental Program in Vascular Biology and Therapeutics with collaborative support from Tarek Fahmy, Ph.D., in the Department of Biomedical Engineering, Yale University School of Medicine. Funding for this research was provided by the Howard Hughes Research Training Fellowship for Medical Students and the Office of Health Science Research Grant from the Department of Surgery at Yale University School of Medicine. I would like to thank Halima Chahboune for her help with the MRI analysis, Naru Hibino and Tai Yi for their help with the scaffold implants, Nancy Troiano for her help with GMA and paraffin embedding, Lesley Devine for her help with Flow Cytometry, Jason Criscione for helpful discussions and Serge Kobsa for his consultation and review of statistical analyses.

Table of Contents

Introduction

Congenital heart defects (CHDs) occur in about 1% of all live births, affecting approximately 40,000 infants in the United States each year, and making CHDs the most common congenital malformation in newborns (1,2). Although many of these defects can be managed medically, there are still a number of complex CHDs that rely on surgical correction to obtain an adequate circulation and to correct structural defects that pose a threat to the normal development of the heart, lungs, and other organs. It is estimated that each year approximately 10,000 children undergo surgical reconstructive operations to repair complex congenital cardiac abnormalities (3,4). While there have been significant advances in the field of pediatric cardiothoracic surgery in the last 20 years that have resulted in well documented reductions in surgical mortality and morbidity, there are still many operations for the more complex CHDs that have shown limited long-term outcome improvements due to the limitations encountered with the use of currently available prosthetic grafts (5).

Congenital heart defects consisting of single ventricle physiology are some of the most severe forms of cyanotic heart disease, nearly universally requiring surgical repair with a Fontan procedure (6). The most widely used surgical technique consists of performing an extracardiac Fontan operation where the venacaval circulation is shunted directly to the pulmonary circulation via an extracardiac conduit (6-9). While this technique has significantly improved the morbidity and mortality associated with repair of this defect, it still has major

drawbacks. The most widely cited disadvantage is the need to use prosthetic conduits, which develop stenosis associated with the somatic growth of the child, have inherent thrombogenic properties, and have a significant potential for infection (6,10). Although the use of prosthetic grafts is life saving in many of these situations, the substantial number of limitations associated with their use poses special challenges for the pediatric population with predisposition of the surgical recipient to repeat operations throughout their life (11).

The field of tissue engineering has provided an alternative solution aimed at addressing many of these issues with the development of tissue engineered vascular grafts (TEVGs). Tissue engineering is a type of regenerative medicine that utilizes the principles of engineering along with the biological sciences to create neotissues that are able to replace, repair, or regenerate damaged tissues (12,13). In vascular tissue engineering, one of the main areas of focus has been the development of autologous TEVGs that have the ability to grow and possess histological and physiological functions similar to those of native tissue. These properties overcome many of the limitations associated with the use of synthetic grafts and their use in the pediatric population would represent a major advancement in the repair of complex congenital heart defects.

Multiple studies have already demonstrated the ability to create tissue-engineered neovessels *in vivo* without any synthetic components that function like native blood vessels (14-16). These TEVGs are based on the classic tissue-engineering paradigm whereby autologous bone marrow mononuclear cells (BMNCs) are harvested and seeded onto biodegradable scaffolds which serve as

extracellular matrices, allowing for cellular adhesion and early structural integrity (17). These structures are implanted in the host's vasculature and, over a course of six weeks, the scaffolds undergo degradation by hydrolysis, resulting in the development of neovessels that have growth potential and resemble the native vasculature in their biochemical, mechanical, and histological properties (18-20). The results from early animal models of TEVG development were so promising that the first clinical application of this technology is already underway at Tokyo Women's Medical University in Japan (21,22). Between September 2001 and December 2004, 25 patients with single ventricle physiology underwent an extracardiac total cavopulmonary connection (TCPC) using a tissue engineered vascular graft. Late-term follow up of this first-in-human clinical study has shown promising results for the continued use of TEVGs to correct congenital heart defects with single ventricle physiology (3,23). As of 2009, the mean follow-up was 5.8 years and, up to this point, there had not been any graft-related deaths. There were six patients that demonstrated asymptomatic graft narrowing, of which four underwent successful balloon angioplasty. In January of 2009, the functional status of all patients was assessed, showing that all surviving patients were attending school or worked regularly, with 17 patients in New York Heart Association functional class I, and 3 patients in functional class II. In anticipation of continued clinical use and an upcoming clinical trial in the United States for which our group has recently obtained FDA approval, the work in our lab has been focusing on delineating the mechanisms of neovessel development with the goal of creating improved, second generation TEVGs.

In order to study the cellular and molecular mechanisms underlying TEVG neovessel formation, our lab developed a murine model that allows for the implantation and evaluation of human cells and tissues in SCID mice. This model has been optimized for neovessel formation with both arterial and venous TEVGs (19,24,25). Our lab has been using this model of TEVG development to better understand the intricate process of neovessel development that occurs after implantation of the seeded scaffold. Before the development of this model, it was known that neovessels form after implantation of a biodegradable scaffolds seeded with bone marrow mononuclear cells; however, the exact mechanisms and requirements for successful development were poorly understood . Until recently, the idea that stem cells and endothelial progenitor cells (EPCs) within the seeded bone marrow population gave rise to the cells of the neovessel was the most widely held belief about the mechanism of neovessel development (17,26). This theory was based on evidence that vasculogenesis could take place beyond the embryonic period through the migration and differentiation of circulating bone marrow derived stem cells or endothelial progenitors at sites of ischemic injury and vascularization (27). Various groups had reported evidence that bone marrow derived endothelial progenitor cells circulate in the blood of adult organisms and that mature endothelial cells can be derived by culturing and differentiating various bone marrow populations (28-30). Clinical investigations provided evidence that mobilization of EPCs was increased in models of ischemia (29), as well as that the transplantation of bone marrow progenitors led to increased blood flow in ischemic injury (31,32). It was reported that the use of bone marrow cells in vascular tissue

engineering increased endothelialization, and it was thought that the BMCs differentiated into the endothelial and smooth muscle cells of tissue engineered vascular grafts (17,26).

Several recently published studies from our lab have provided evidence arguing against this school of thought. First of these came from tracking the fate of seeded human bone marrow-derived mononuclear cells (hBMCs) in our immunodeficient mouse model of TEVG development through serial post-implantation monitoring with histology and PCR that showed a complete loss of human cells within the TEVGs after one week (33). This evidence was further supported by subsequent work in our laboratory tracking the fate of seeded syngeneic bone marrow-derived mononuclear cells labeled with GFP in an immunocompetent mouse model, which similarly showed the rapid loss of cells by GFP DNA quantification (unpublished data). In both instances, the loss of the seeded BMCs was accompanied by a rapid infiltration of host monocytes/macrophages and, eventually, by host endothelial and smooth muscle cells. This provides further evidence that neovessel formation occurs through a process of inflammatory vascular remodeling where the seeded BMCs act in a paracrine manner to recruit host inflammatory cells (33). Similar findings by other groups also provide evidence that BMCs are necessary for neovascularization by acting in a paracrine manner and not by directly incorporating into the neovasculature (34,35).

While the evidence is plentiful to support this new hypothesis about the origin of cells that give rise to neovessels, the methods that were used to perform these experiments highlight one of the major limitations in the field of tissue

engineering – the paucity of available tools for noninvasive cell tracking that allow repeated observations of a single tissue-engineered vessel as it undergoes dynamic changes. To date, most *in vivo* experiments designed to study the mechanism of neovessel development on the molecular and cellular level have required sacrificing the animals at each observation point in order for the tissue to be harvested for analysis, and thus precluding the ability to perform longitudinal observations in a single animal (36). In this study, we use cellular MRI to track the fate of seeded cells in a longitudinal model through serial imaging, providing first such evidence to our knowledge by utilizing a noninvasive approach to study the mechanism of neovessel development. As a result of rapid progress being made in several areas of tissue engineering, noninvasive longitudinal monitoring is becoming increasingly more important in clinical trials that require non-invasive techniques for monitoring and investigating cell therapies and neotissue development in host organisms. Such noninvasive methods drastically decrease the number of required subjects and associated costs, as well as open the door to human trials. Specifically, MRI is being used to advance this research through noninvasive monitoring of tissue structures, composition and function, in order to improve the tissue engineers' ability to direct the process of neotissue development (37).

MRI has been the chosen imaging modality for accomplishing this because of its ability to depict tissues with greater spatial resolution than other clinical imaging modalities (38,39). MRI is further greatly enhanced with the use of targeted contrast agents, giving it ability for near cellular resolution (40,41), as well as whole-body imaging capability without ionizing radiation (42-47). MRI has the capability of

imaging slices in any orientation, at any depth, with a resolution of approximately 100 μm (37). Other imaging modalities such as optical and fluorescent microscopy and micro-CT have been used in tissue engineering, but each comes with limitations. Intravital two-photon fluorescence microscopy has been used to track fluorescently labeled cells in tissue, but is not ideal for routine investigations in mice because of its invasive nature and its ability to only image exposed or superficial explanted tissue (48-50). Micro-CT has the ability to penetrate deeply into tissues, but uses ionizing radiation and, in order to provide adequate contrast, requires dense tissue (37). Similarly, single-photon emission computed tomography and positron emission tomography are able to penetrate deeply into tissue, but use radioactive labels that can adversely affect living cells (51,52). MRI overcomes all of these limitations, has the potential for imaging deep into tissue with high sensitivity and spatiotemporal resolution with the ability to follow dynamic changes as the tissue-engineered constructs develop (53). In addition, no other imaging modality with whole body imaging capability has shown single-cell *in vivo* cell-tracking ability (40).

In order to perform *in vivo* cell tracking, targeted contrast agents are used to label cells. To date, dextran coated superparamagnetic iron oxide (SPIO) nanoparticles have been used as the leading contrast agents for cell tracking purposes. The SPIO particles are distinguished based on their size after coating as SPIO particles with a diameter of 50-150 nm, ultrasmall superparamagnetic iron oxide nanoparticles (USPIO) with a diameter less than 50 nm, and micron size paramagnetic iron oxide particles (MPIO)(54). They are currently the most widely

used contrast agents for cell tracking because MRI has greater sensitivity for superparamagnetic agents over paramagnetic agents such as gadolinium- based agents which suffer from an inherently high threshold of detectability (55,42,47,56). In addition, superparamagnetic agents are iron based and therefore benefit from a low level of cellular toxicity. Multiple studies have shown that SPIO particles do not adversely affect cell viability, physiology, differentiation, or migration ability (54,57). These properties explain why it is currently the most widely used agent in the fields of cellular and molecular MRI.

The fields of cellular and molecular MRI, which can be defined as the "non-invasive and repetitive imaging of targeted cells or macromolecules in living organisms," (55) are two relatively new and rapidly growing fields that have the potential to allow deeper insight into the underlying *in vivo* biology of many systems and cellular processes without disturbing the native system dynamics. To date, most uses of non-invasive cellular imaging have been focused on macrophage imaging in a wide range of applications including tumor staging, atherosclerotic change visualization, and inflammatory CNS disease (58-62). This predominantly arises from the ease of labeling phagocytic cells with contrast agents, the preferential phagocytosis of SPIO nanoparticles by monocytes and macrophages *in vivo*, and the large cell numbers that accumulate at sites of inflammation that help overcome detection limitations (54). In addition to macrophage imaging *in vivo*, several research groups are beginning to use *ex vivo* labeling of various cell types with subsequent injection and cell tracking *in vivo,* as well as SPIO nanoparticles that are conjugated to target-specific ligands (63,64). A few recent applications of cellular

tracking utilizing MRI and SPIO-labeled cells include visualizing neural stem cell migration to cortical inflammatory lesions, monitoring transplanted pancreatic islets, and monitoring mesenchymal stem cells transplanted into infarcted myocardium (65-67).

The available studies are even more limited with respect to molecular MRI (mMRI). Molecular MRI uses MRI contrast agents as probes by linking them to specific monoclonal antibodies that are targeted to specific receptors or antigens. The most recently published work in this field is by Towner *et al.* (68) and involves using magnetite-based dextran-coated nanoparticles covalently bound to VEGF-R2 antibodies that serve as mMRI probes to detect *in vivo* levels of VEGF-R2 as a marker of angiogenesis in gliomas. MR images of glioma-bearing rat brains appeared hypodense at the location of gliomas in animals injected with the iron-oxide nanoparticle probes, compared to control mice injected with regular antibodies. The authors concluded that this showed the feasibility of using mMRI to assess angiogenesis in an *in vivo* model and that this could easily be extended to the field of vascular tissue engineering.

Similarly to most of the research in other fields, the most widely used contrast agents for cellular MRI in tissue engineering applications are based on labeling cells with superparamagnetic iron oxide nanoparticles. During the last five years most applications have predominantly consisted of enhancing seeding techniques and visualization of cell seeding efficiency and distribution both *in vitro* and *in vivo* (69-72). Perea *et al.* (69) labeled human umbilical vein endothelial cells (HUVECs) with SPIO nanoparticles and then used an electromagnet to direct cell

seeding onto the lumen of a polytetrafluoroethylene (PTFE) tubular graft with subsequent visualization by MRI to analyze cellular distribution. Shimizu *et al.* (70) described another technique referred to as Mag-seeding in which NIH/3T3 fibroblasts (3T3s) were labeled with magnetite cationic liposomes (MCLs) and then seeded onto a decellularized porcine common carotid artery by inserting a cylindrical magnet into the lumen of the artery and then submersing the unit into a suspension of labeled 3T3s. Wilhelm *et al.* (73) was able to show that the formation of vascular networks could be directed in Matrigel models of *in vitro* vascularization by using a magnetic field to move magnetically labeled endothelial progenitor cells. Most recently, published data by Poirier-Quinot *et al.* (74) demonstrated the potential of using a high resolution 1.5-T MRI for noninvasive 3D visualization of tissue engineered scaffolds seeded with iron oxide labeled mesenchymal stem cells (MSCs) both before and after implantation subcutaneously in mice. They proved the feasibility of using high-resolution 1.5-T MRI to visualize the architecture of their scaffolds and to study and characterize 3-dimensional cell seeding both *in vitro* and after subcutaneous scaffold implantation. This represents a proof-of-principle study that shows the feasibility of using this technique to follow longitudinal cell migration from the time of scaffold implantation both throughout the scaffold itself and from the scaffold to other areas of the body. This is the direction the field of cellular MRI is progressing in tissue engineering applications.

Recently, there have been more studies in the literature that have advanced beyond using iron oxide nanoparticles to simply enhance cell seeding techniques to explore the usefulness of cellular MRI for tracking the fate of cells seeded onto

scaffolds intended for tissue regeneration. While most of these studies are based on *in vitro* work, there have been several investigations that have utilized *in vivo* approaches to demonstrate the feasibility of using this technology to advance our understanding of the dynamic changes occurring post-implantation. Terrovitis *et al.* (75) was one of the first groups to look at the possibility of using cellular MRI to visualize SPIO-labeled human mesenchymal stem cells (MSCs) seeded onto 1% type I bovine collagen scaffolds intended for use as tissue-engineered heart valves. They labeled MSCs with ferumoxide nanoparticles, demonstrated that the cell labeling did not cause adverse effects on the cells, and then showed by *in vitro* T2 weighted MRI that the labeled cells seeded onto the scaffolds could be visualized as areas of reduced signal intensity with a 40-50% shorter T2 relaxation time than similar unlabeled cells. This was one of the first studies to show the promise of using these techniques for cell tracking in future tissue-engineering applications.

Heymer *et al.* (76) performed a similar study looking at the feasibility of using very small superparamagnetic iron oxide particles (VSOPs) to label MSCs for the purpose of creating a reliable cell monitoring technique in articular cartilage repair. They labeled MSCs with the VSOPs, demonstrated that cell viability was not affected, and then performed high-resolution MRI of the VSOP-labeled MSCs embedded in a clinically used collagen type I hydrogel. Similarly to Terrovitis *et al.,* this study was performed entirely *in vitro* and demonstrated the potential for using MRI to track the migration of the VSOP-labeled cells post-implantation.

The first *in vivo* applications of these methods have been published recently and consist mostly of demonstrating the ability to visualize the labeled cells

immediately after scaffold implantation. Saldanha *et al.* (77) demonstrated the ability to visualize ferumoxide-labeled MSCs in an *ex vivo* rat model of a tissue engineering based approach to the regeneration of the intervertebral disc. Ferumoxide-labeled MSCs were loaded into polyethylene glycol hydrogels and imaged *in vitro,* verifying the ability to detect the labeled cells on T2-weighted MRI through signal intensity loss. Next, labeled cells were loaded into fibrin gels and injected into the intervertebral disc spaces of excised rat tails and imaged. It was shown that discs injected with the ferumoxide labeled cells appeared darker on T2 weighted images than discs injected with fibrin gel alone. The authors concluded that this provided the potential for *in vivo* longitudinal tracking of MSCs in the tissue engineering based approach to intervertebral disc regeneration. Ko *et al.* (78) went one step further by monitoring gelatin sponges seeded with SPIO-labeled MSCs that were implanted subcutaneously in the hind limbs of nude mice. Serial MRIs were performed over a period of 4 weeks demonstrating the ability to visualize the gelatin sponge containing the SPIO-labeled MSCs as a hypodense region in the hind limbs of the animals. They concluded that the area of hypodensity increased over the 4-week period as the seeded MSCs spread out from the implanted gelatin sponges. This represents one of the first published works verifying the ability to use cellular MRI to track seeded cells in an *in vivo* tissue engineering model. Although this study was using a quasi-tissue engineering product and was not focused on a specific tissue engineering application, it still laid the foundation for using SPIO cell labeling and cellular MRI for *in vivo* longitudinal cell tracking in tissue engineering applications.

One of the first studies that applied SPIO cell labeling and MR cell tracking to a specific tissue engineering application was performed in our laboratory by Nelson *et al.* (79) in the field of vascular tissue engineering. Nelson *et al.* conducted a pilot study using human aortic smooth muscle cells (hASMCs) labeled with ultrasmall superparamagnetic iron oxide nanoparticles (USPIOs) that were seeded onto tissue engineered vascular grafts (TEVGs) and implanted as aortic interposition grafts in C.B.-17 SCID/bg mice. Mice were then imaged at different time points over a 3-week period demonstrating that the TEVGs seeded with USPIO-labeled cells appeared darker on T2 weighted images than unseeded scaffolds. It was concluded that USPIO cell labeling enhanced visualization of the tissue engineered vascular constructs *in vivo,* demonstrating the feasibility of applying noninvasive MR cell tracking techniques for evaluation of *in vivo* TEVG performance.

There have not been any studies in the field of vascular tissue engineering that have utilized cellular MRI to answer questions regarding the process of neotissue development once the tissue engineered constructs are implanted. A study of this nature would require serial imaging of labeled cells in a live animal model of vascular tissue engineering. The studies previously mentioned have set the background for utilizing this technology to answer such questions from a noninvasive standpoint, instead of current methods that require the tissue engineered constructs to be excised, usually terminating the animals for analysis. Given our interest in clinical applications of TEVGs in congenital cardiac defect repairs, which typically occur in the low pressure venous system, in this study we sought to demonstrate our ability to serially track USPIO-labeled macrophages

seeded onto our TEVGs after they are implanted as interposition grafts in the inferior vena cavas of SCID/bg mice for the purpose of determining the fate of seeded cells and their role in venous neovessel formation.

In order to achieve this, murine macrophages were labeled with USPIO through *in vitro* culture in media containing USPIO. The USPIO-labeled macrophages were seeded onto polyglycolic acid (PGA) scaffolds that were surgically implanted as inferior vena cava interposition grafts in SCID/bg mice. Images were then obtained on a 4.7T Bruker horizontal bore scanner with an optimized RARE spin echo sequence and a multislice-multiecho sequence to determine T2 relaxation time with serial imaging. The signal intensities were verified using Prussian blue staining for iron containing macrophages. To our knowledge, this is the first study performed in vascular tissue engineering that utilizes serial MR imaging of a TEVG in a live animal model to study neovessel development on a cellular level.

Statement of Purpose

The overall aim of this project is to utilize cellular MR imaging to noninvasively track the fate of cells seeded onto tissue engineered vascular grafts (TEVGs) after *in vivo* implantation. We hypothesize that the seeded cells will be rapidly lost from the implanted scaffold and that this loss will be detected by an increase in T2 signal. In order to accomplish this, we will optimize the conditions for labeling macrophage populations with USPIO nanoparticles. After labeling conditions have been determined not to affect cell viability, we will determine the limit of detection of the labeled cells and verify the ability to visualize the labeled cells on TEVGs *in vitro.* Finally we will implant USPIO-labeled scaffolds as Infrarenal IVC interposition grafts in SCID/bg mice and perform serial MR imaging and T2 mapping to track the fate of the seeded cells.

Materials and Methods

Biodegradable Scaffolds

Scaffolds were constructed from a nonwoven polyglycolic acid (PGA) mesh felt (ConcordiaFibers, Coventry, RI, USA) and coated with a 50:50 co-polymer sealant solution of poly-L-lactide and ε-caprolactone (P(CL/LA)). The PGA mesh felts were shaped into tubes by introducing 6.0 x 6.0 mm sections into the inlet of a cylinder with an internal diameter of 1.4mm. Stainless steel 21-gauge needles were then introduced into the opposing end to maintain the inner lumen and compress the felt. A 5% (w/v) P(CL/LA) (263.8 kDa; Absorbable Polymers International, Birmingham, AL, USA) in dioxane sealant solution was injected into the inlet of the chamber system and allowed to penetrate the felt. The scaffolds were then frozen at –20°C for 20 min and lyophilized for 24 hours. This resulted in PGA-P(CL/LA) scaffolds with an internal diameter of 0.9 mm.

(Scaffolds were made by Jamie K. Harrington)

Cell Culture

Murine macrophages (Cell Line Raw 264.7 (ATCC®) were cultured in RPMI Media 1640 containing 10% (vol/vol) FBS and 1% (vol/vol) Penicillin/Streptomycin (GIBCO®). Cells were harvested between passages 3 and 6 for all experiments.

(Performed by Jamie K. Harrington)

Incubation of Murine Macrophages with USPIO Nanoparticles

Commercially available USPIO nanoparticles (Molday ION (-) Biophysics Assay Laboratory, Inc, Worcester, MA) were supplied in 2 ml sterile sealed serum bottles with a concentration of 10 mg Fe/ml. This stock solution of USPIO nanoparticles was diluted directly into murine macrophage serum free culture media (SFM) (RPMI-1640 with 1% (vol/vol) Penicillin/Streptomycin, GIBCO®) for all experiments. Murine macrophages were incubated at an optimized USPIO concentration of 2 mg/ml for 36 hours in SFM.

(Performed by Jamie K. Harrington)

Coating USPIO Nanoparticles with Poly-l-lysine

In some experiments, the USPIO nanoparticles were pre-incubated with a solution of high molecular weight poly-L-lysine (Sigma-Aldrich, St. Louis, MO, USA) in order to enhance uptake. 30 mg of Combidex nanoparticles were added to 15 ml of serum-free high-glucose Dulbecco's modified Eagle medium (DMEM; Invitrogen, Carlsbad, CA, USA). This solution was mixed with 1.8 mg of poly-l-lysine dissolved in 15 ml of high-glucose DMEM for 1 h on an orbital shaker, which produced 30 ml of stock solution containing USPIO and poly-l-lysine concentrations of 1000 μg/ml and 60 μg/ml, respectively. This ratio of USPIO to poly-l-lysine was held constant throughout all serial dilution studies.

(Performed by Jamie K. Harrington)

Prussian Blue Staining and Labeling Efficiency Determination

Prussian Blue staining for intracellular iron was performed on macrophages incubated with USPIO nanoparticles to determine the labeling efficiency. Macrophages were incubated for 36 hours with a 2 mg/ml concentration of USPIO nanoparticles. Following the incubation period, the cells were washed 3 times with PBS, trypsinized, and plated onto sterile microscope coverslips. Once adherent, the cells were fixed in 10% neutral buffered formalin (NBF; Sigma-Aldrich) overnight and stained for the presence of intracellular iron. Potassium ferrocyanate (4% w/v in distilled water) was mixed with a 20% w/v solution of hydrochloric acid right before use. The cells were then exposed to this mixture for 20 minutes before being washed 3 times with distilled water. Cells were then counterstained with nuclear fast red counterstain (Sigma-Aldrich) at room temperature for 5 minutes. Labeling efficiencies were determined by counting the fraction of cells staining positive for Prussian blue. Macrophages receiving no USPIO served as controls negative controls and spleen tissue sections served as positive controls.
(Performed by Jamie K. Harrington)

Cell Metabolism Assay

In order to determine macrophage metabolic activity following USPIO labeling, a CellTiter 96® AQueous Non-Radioactive Cell Proliferation Assay (MTS) (Promega Corporation, Madison, WI, USA) was performed. Macrophags were incubated for 36 hours with 2 mg/ml of USPIO nanoparticles. Following the incubation period, the cells were washed 3 times with PBS and the assay reagent (tetrazolium

compound(3-(4,5-dimethylthiazol-2-yl)-5-(3-carboxymethoxyphenyl)-2-(4-sulfophenyl)-2H-tetrazolium, inner salt; MTS) and an electron coupling reagent (phenazine methosulfate; PMS)) was added to the cells at an 1:4 ratio with media and allowed to incubate for 4 hours at 37C. After 4 hours, a 100 µl aliquot of each sample was added to a clear 96-well plate and the absorbance at 490 nm was read. The relative cell metabolic activity was determined as the ratio of absorbance from wells incubated with USPIO to the control wells (receiving no USPIO). Experiments were performed in triplicate.

(Performed by Jamie K. Harrington)

Flow Cytometry

In order to determine macrophage cell viability after USPIO labeling, 7-aminoactinomycin D (7-AAD) Flow Cytometry was performed and compared to macrophages receiving no USPIO concentration. For flow cytometry, cells were pipetted up and down several times to remove attached cells and to break up clumps. Cells were then passed through a 100 µm cell strainer and transferred to 5 ml polypropylene tubes (BD Bioscience, San Jose CA). After centrifugation to pellet cells (200 x g for 10 minutes), cells were resuspended in 100 µl staining buffer (PBS with 1% fetal bovine serum and 0.1% sodium azide). To assess viability, 20 µl of Viaprobe (BD Bioscience) was added to each tube and incubated on ice for 10 minutes. Next, 200 µl of staining buffer was added and the cells were analyzed on a FACSAria cell sorter (BD Bioscience). Results were analyzed using Flowjo (Tree Star Inc. Ashland, OR). Experiments were performed in triplicate.

(Performed by Lesley Devine in Laboratory Medicine)

Macrophage Seeding of Polymer Scaffolds

Each PGA-P(CL/LA) scaffold was trimmed to 4 mm in length and sterilized via incubation at 20°C under UV light in sterile PBS. Scaffolds were washed in sterile PBS prior to seeding. Macrophages were trypsinized and collected for seeding in RPMI-1640 media. Approximately $5x10^6$ cells were statically seeded onto each scaffold by directly pipetting the cell suspension into the lumen through both ends. The scaffold was then gently compressed to encourage cell infiltration into the porous walls. This process of pipetting and compression was repeated 3 times at each end of the scaffold. Each seeded scaffold was then allowed to sit for 15 min to allow cell adhesion. A 21-gauge needle was then gently threaded through the lumen of the graft to prevent occlusion via cellular ingrowth and each graft was incubated overnight in 3 ml of RPMI-1640 media.

(Performed by Jamie K. Harrington)

Seeding Efficiency Determination

Prior to *in vivo* application, it was important to determine if the seeding efficiency of the USPIO labeled macrophages on the scaffolds was sufficient to be detected by MRI. Various numbers of USPIO-labeled macrophages ($1x10^6$, $5x10^6$, $10x10^6$, and $15x10^6$) were statically seeded onto biodegradable PGA-P(CL/LA) scaffold constructs as previously described. Seeding efficiency was then determined by measuring the DNA content on the scaffolds with the PicoGreen detection assay (Quant-iTTM PicoGreen® dsDNA Assay Kit, Molecular Probes Inc, Eugene, OR)

following a 24 hour incubation. After the 24 hour *in vitro* incubation, the seeded scaffolds were rinsed 3 times in PBS, placed in 200 µL of distilled water, and stored at -80°C for a minimum of 24 hours. At the time of evaluation, scaffold sections were thawed at 37.8°C. A black 96-well plate was loaded with 50 µL from each sample. A 30 µl aliquot of the PicoGreen dye was mixed thoroughly with 6 ml of Tris-EDTA buffer (pH 7.5) and 50 µl was added to each sample in the 96-well plate. All samples were performed in triplicate. The plate was incubated in the dark at room temperature for 10 minutes. Fluorescence was measured at 488 nm excitation and 525 nm emission. The number of cells maintained on each scaffold was determined from a standard curve generated from a known quantity of macrophages. A negative control of unseeded scaffold sections was used for comparison.

(Performed by Jamie K. Harrington)

MRI

All MRI experiments were performed on a 4.7T Bruker horizontal-bore system with custom-made bird cage coils.

(All MRI samples were prepared for MRI by Jamie K. Harrington; The MRI sequences were run by Halima Chahboune in the Biomedical Engineering Department; The scaffold implants were performed by Naru Hibino and Tai Yi in the Interdepartmental Program in Vascular Biology and Therapeutics; Anesthesia was performed by Jamie K. Harrington)

In vitro MRI

To determine the minimal quantity of detectable cells, decreasing numbers of labeled cells ($25x10^6$, $20x10^6$, $15x10^6$, $10x10^6$, $5x10^6$, and $1x10^6$), and unlabeled cells were imaged. For T2-weighted images a spin-echo (SE) sequence was used with the following parameters: TR/TE = 3000/20 ms; matrix size= 128×128; FOV = 32×32 mm; slice thickness = 1mm; number of slices = 3. For T2 maps, the images were acquired using a multispin multiecho (MSME) with the following parameter: TR/TE= 3000/18 ms, number of echoes=8 with TE spacing =18ms, matrix size= 128×128; FOV = 32×32 mm; slice thickness = 1mm. The image intensities, T2 maps and values were obtained using home-written Matlab (Natick, MA) software.

To verify the potential of cell tracking on a clinically relevant substrate, biodegradable scaffolds seeded with USPIO labeled macrophages and controls were imaged using the same MRI sequences above. The controls consisted of a scaffold seeded with unlabeled macrophages and an unseeded scaffold.

Cell Labeling and Suspension

In order to determine the cellular limit of detection of USPIO-labeled macrophages MRI phantom imaging of known numbers of labeled cells was performed. Macrophages were grown to confluency in a T75 flask and incubated with 2 mg/ml of USPIO nanoparticles for 36 hours in SFM. Labeled cells were then collected, counted, and fixed in 10% neutral buffered formalin (NBF; Sigma-Aldrich) overnight. Following fixation, labeled cells were homogenously suspended in Histogel® (Richard-Allan Scientific, Kalama- zoo, MI, USA) in the following known

quantities: $25x10^6$, $20x10^6$, $15x10^6$, $10x10^6$, $5x10^6$, and $1x10^6$. The known cell numbers were suspended in 500 µl of PBS using Corning® 96 Well Polypropylene Cluster Tubes and then 500 µl of Histogel was added pipetting up and down to ensure the cells were homogenously suspended. Controls consisted of samples without cells and samples with unlabeled cells.

The cellular limit of detection was determined by analyzing the T2 maps of the cellular suspensions. The number of cells in each 1 mm slice of the homogenous cell suspension was determined by calculating the volume of the cylindrical tube used for the MRI (height = 1 mm, radius = 3.5 mm). This number corresponded to a given T2 value for each sample.

Scaffold Suspensions

Prior to *in vivo* application, it was important to image a TEVG seeded with USPIO labeled macrophages in order to confirm the potential for cell tracking on a clinically relevant substrate. Biodegradable scaffolds were seeded with USPIO labeled macrophages and unlabeled macrophages as previously described. On day 1 post seeding, the seeded scaffolds were suspended in Histogel (BD Biosciences, San Jose, CA, USA) in Corning® 96 Well Polypropylene Cluster Tubes. As controls, one tube was filled with Histogel and one contained an unlabeled scaffold. MR imaging was performed as described above.

In vivo MRI

For *in vivo* MRI, Mice with seeded labeled or seeded unlabeled scaffolds were anesthetized with 1.5 % isoflurane and imaged immediately after the implantation every 30 min for 9 h. On post-operative day 7, mice were again anesthetized and maintained on isoflurane for imaging. For T2 weighted images, the images were acquired using a rapid acquisition with relaxation enhancement spin-echo sequence (RARE). Imaging parameters were as follows: field of view = 28 mm, image matrix = 128 × 128, slice thickness = 1 mm, RARE factor = 4, effective echo time = 34 ms and recycle time = 4 s. For T2 maps, (MSME) sequence was used with the following parameters: Number of echoes=6 and echo spacing =17 ms, TR/TE =4000/17 ms, field of view = 28 mm, image matrix = 128 × 128, slice thickness = 1 mm. T2 maps were generated by pixel-by pixel fitting using home-written Matlab 6.5.2 (The Math Works, Inc, USA)

Implantation of Biodegradable Scaffolds

Anesthesia was induced by inhalation of 4% vaporized isoflurane in a mixture of oxygen. During surgical procedure, isoflurane was maintained in 0.5-1.5 % without any clinical signs of pain or changes of macrohemodynamic parameters. For the animals undergoing surgery for postmortem MR analysis, xylazine/ketamine anesthesia was used instead. These animals were anesthetized with intraperitoneal injection made by mixing 1.5 ml of 100 mg/ml xylazine (Sigma-Aldrich) and 10 ml of 100 mg/ml ketamine (Sigma- Aldrich) diluted in a ratio of 1:4 with 0.9% normal

saline and injected at a dose of 0.1 ml/20 g of body weight. Upon induction of anesthesia the animals were placed in a supine position. Using an X18 dissecting microscope (Zeiss, Thornwood, NY, USA), a midline laparotomy was performed, and the abdominal viscera were lateralized to allow visualization of the abdominal aorta. Care was taken to separate the aorta from the vena cava. Proximal and distal vascular control of the vessels was obtained below the renal vessels and above the iliac bifurcation. The open abdominal cavity was bathed in warmed (37°C) heparinized saline (250 U/ml). The native vessel was gently occluded with removable microvascular clamps and then transected. Anastamosis to a caliber-matched TEVG (1 mm diameter) was performed at the infrarenal level of the IVC using interrupted 10-0 monofilament nylon (Sharpoint Lab Sutures, Calgary, AB, Can- ada). On completion of the distal anastamosis, the midline incision was closed with running 5-0 prolene sutures. After laparotomy closure, animals were monitored during recovery and placed on a warm pad to avoid hypothermia. The animals recovered from surgery and were maintained without the use of any anti-coagulation or anti-platelet therapy.

Animal handling was in accordance with the institutional guidelines for the use and care of animals, and the institutional review board approved the experimental procedures.

Postmortem MR imaging

Postmortem imaging was performed with USPIO labeled scaffold implants immediately after implantation and one-week post-implantation as proof of

principle for serial imaging. USPIO-labeled and unlabeled macrophages were seeded onto biodegradable polymer scaffolds that were then implanted as interposition grafts in the Inferior Vena Cavas (IVC) of female C.B-17 SCID/bg mice. Two mice with USPIO-labeled scaffold implants and two mice with unlabeled scaffold implants were euthanized by CO_2 asphyxiation immediately following surgical implantation and underwent postmortem imaging. Two mice with USPIO-labeled scaffold implants and two mice with unlabeled scaffold implants were resuscitated after the surgical implantation and euthanized 7 days later for postmortem imaging.

Histologic analysis

All infrarenal IVC scaffolds were explanted and fixed in 10% neutral buffered formalin (NBF; Sigma-Aldrich) overnight prior to histological embedding with glycolmethacrylate (GMA). GMA-embedded samples were stained with Lee's methylene blue (a substitute for traditional hematoxylin and eosin (H&E) staining) with a nuclear red counterstain. Scaffolds were stained for the presence of intracellular iron with Prussian blue as previously described.
(Scaffold explantation and tissue fixation was perfomed by Jamie K. Harrington; Sample embedding was performed by Nancy Troiano; Tissue staining was performed by both Jamie K. Harrington and Nancy Troiano)

Cell Counting

Two separate sections of each scaffold explant were stained with H&E and Prussian blue and imaged at a magnification of 400x. The number of nuclei were counted in four regions of each section and averaged to determine total cellularity. The number

of cells staining positive for Prussian blue were counted in four regions of each section and averaged to determine total number of cells containing USPIO nanoparticles.

(Performed by Jamie K. Harrington)

Statistical Analysis

Statistical differences were analyzed with paired and unpaired Student's t tests or ANOVAs. $P < 0.05$ was considered statistically significant.

(Performed by Jamie K. Harrington)

Results

Optimization of Macrophage Labeling with USPIO and Scaffold Seeding

Raw 264.7 murine macrophage/monocyte cell line was utilized for all experiments based on prior analysis by our lab showing that the bone marrow cell population used for scaffold seeding is composed predominantly of monocytes (33) and well-established evidence that macrophages are ideal for MRI contrast cell labeling and *in vivo* cell tracking (80-82).

The first objective of this study was to determine an optimal condition to achieve adequate *in vitro* cell labeling of the macrophage cell line. In order to determine these conditions, macrophages were incubated with various concentrations of both poly-l-lysine and non-poly-l-lysine coated USPIO nanoparticles for various incubation durations (data not shown). Based on labeling efficiency determination and cellular and metabolic viability studies the conditions were optimized using non-poly-l-lysine coated USPIO nanoparticles at a concentration of 2 mg/ml for an incubation duration of 36 hours in serum free culture medium (SFM). Serum free culture medium was used for all studies based on evidence that proteins in the serum chelate the iron oxide particles and interfere with cellular uptake e(80). After cell labeling at these conditions Prussian blue staining to reveal intracellular iron deposits consistently showed a robust labeling efficiency (Figure 1A, B).

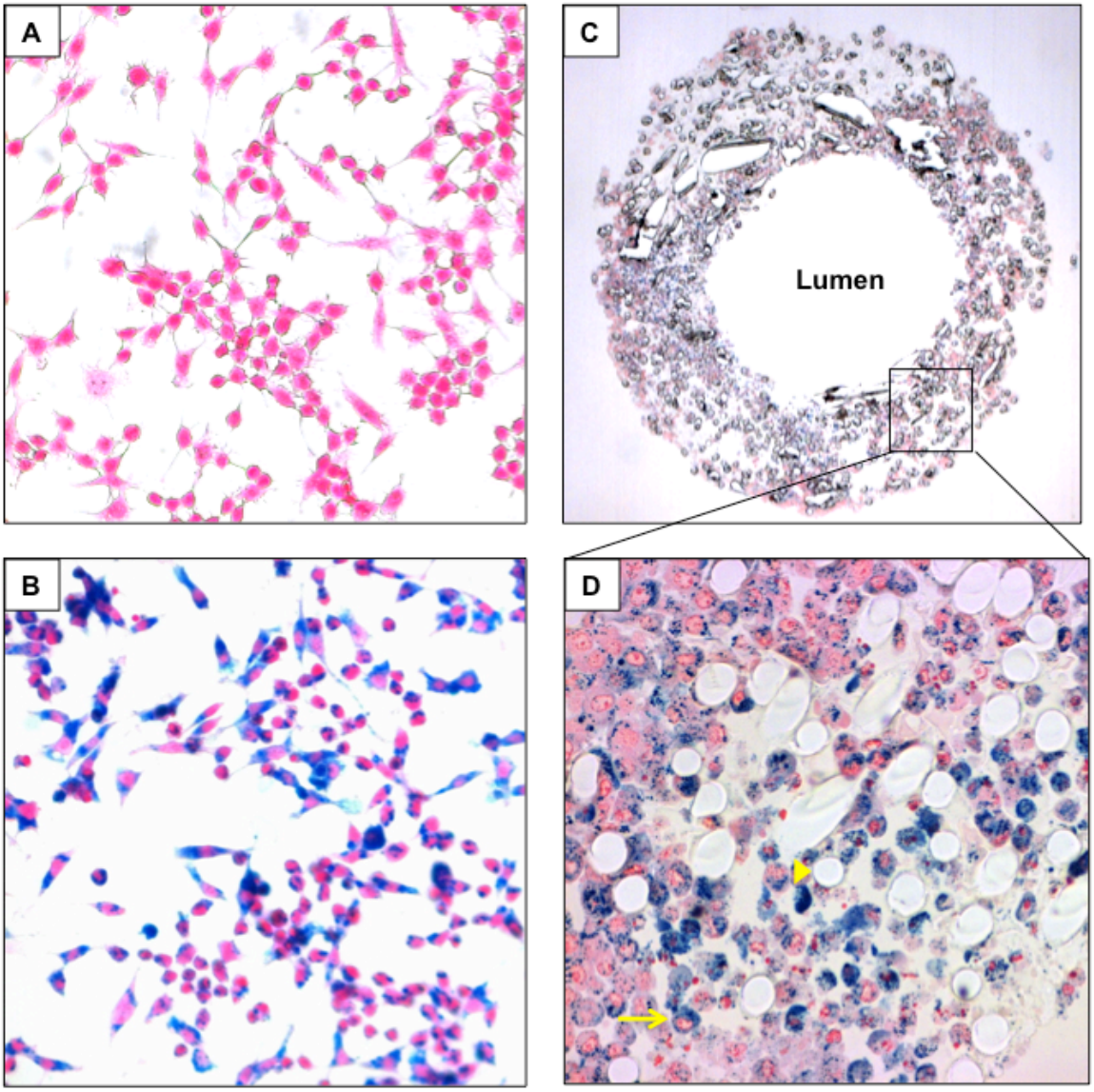

Figure 1. Evaluation of USPIO cell labeling and scaffold cell seeding. Murine macrophages were stained with prussian blue to identify intracellular iron. (A) Photomicrograph of unlabeled control macrophages (H&E, 400x) (B) Photomicrograph of macrophages after USPIO cell labeling (H&E, 400x). (C) Photomicrograph of USPIO labeled macrophages statically seeded onto a biodegradable scaffold (Lee's methylene blue, 40x). (D) Representative section of the same seeded scaffold showing the PGA scaffold fibers (arrowhead) and the USPIO-labeled macrophages (arrow) (Lee's methylene blue, 400x).

The metabolic activity and the cellular viability of the labeled macrophages as measured using the MTS assay and Flow Cytometry, respectively, were not

statistically different from control macrophages (receiving a USPIO concentration of 0 mg/ml) (Table 1).

Table 1. Cell viability and Metabolic Activity of USPIO-labeled macrophages

USPIO Concentration	2 mg/mL	0 mg/mL	p-value
Metabolic Activity (n= 6)	2.99 ± 0.10	3.22 ± 0.06	0.08
Cellular Viability (n= 7)	63.58 ± 0.89	62.99 ± 2.37	0.82

Values are expressed as the mean ± SEM.

Once robust cell labeling was achieved without affecting cellular metabolism or viability, the static seeding efficiency of the USPIO-labeled macrophages onto our PGA biodegradable polymer scaffolds was determined. The static seeding efficiency for the macrophage cell line was found to be approximately 8%. This is consistent with other studies that consistently show a seeding efficiency between 5-10% depending on the cell line being used (72). With this seeding efficiency, five million macrophages could be statically seeded onto each scaffold resulting in retention of approximately 3.8×10^5 ± 13% cells. This was found to be optimal for all experiments. Histological sections of the scaffolds after static seeding and cell culture with the USPIO-labeled macrophages showed the seeded macrophages were able to penetrate the pores of the PGA mesh and were able to remain well infiltrated into the walls and attached to the lumen and exterior of the scaffolds even after scaffold manipulation (Figure 1C, D).

In vitro MRI Analysis

The next objective in the study was to perform an *in vitro* characterization of the USPIO-labeled macrophages and the USPIO-labeled macrophage seeded scaffolds by MR imaging. Labeled macrophages were homogeneously suspended in Histogel® in seven serial dilutions from $25x10^6$ to 0 cells per 1 mL of Histogel® suspension. T2 weighted-images were then acquired using a spin-echo sequence. As the number of labeled cells increased, the T2 signal intensity dropped (Figure 2A) and the T2 values gradually decreased (Figure 2B and Table 2).

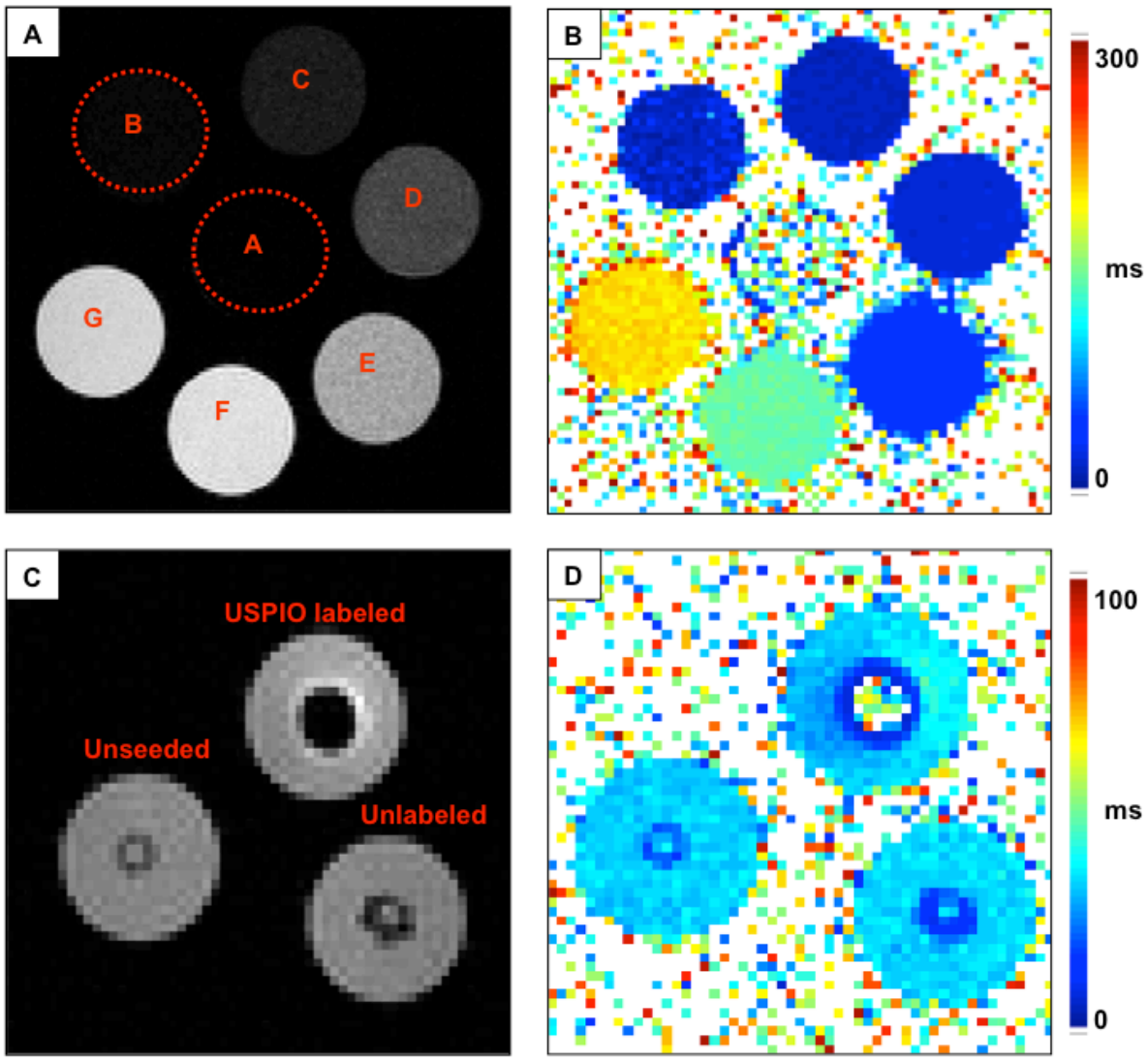

Figure 2. *In vitro* Characterization of USPIO-labeled macrophages and seeded scaffolds. (A) T2 weighted image of a gelatin phantom using an array of concentration gradients of USPIO labeled macrophages: A= $25x10^6$, B= $20x10^6$, C= $15x10^6$, D= $10x10^6$, E= $5x10^6$, F= 10^6 and G= 0 labeled cells (B) T2 mapping of the same sample. (C) *In vitro* T2 weighted image of an unlabeled scaffold, unseeded scaffold and a USPIO-labeled scaffold suspended in gelatin. (D) T2 mapping of the same sample.

Table 2. *In vitro* T2 values of USPIO labeled macrophages.

Sample	Cell Number in 1 mm slice	T2 Value (ms)
A ($25x10^6$)	882,080	(out of range)
B ($20x10^6$)	705,664	15.4
C ($15x10^6$)	529,248	16.5
D ($10x10^6$)	352,832	22
E ($5x10^6$)	176,416	48
F ($1x10^6$) §	35,283	140
G (Control) §	0	202

§ below the limit of detection

Table 3. *In vitro* T2 values of scaffolds seeded with USPIO labeled macrophages.

Scaffold	T2 Value (ms)
USPIO-Labeled	26.66
Non-USPIO-Labeled	45.38
Unseeded	84.5

USPIO is a T2 contrast agent that shortens T2 relaxation times resulting in a negative image with a hypodense signal, resulting in a darker appearance of the image with increasing amounts of iron-oxide in the sample. The T2 values were calculated for each 1 mm slice and based on known cell numbers in each 1 mm MRI slice, the T2 value could be correlated with a given number of USPIO labeled macrophages. The T2 values ranged from 202 ms for the gelatin phantom without any USPIO labeled macrophages to 15.4 ms for the sample with $20x10^6$ macrophages (the sample with the highest amount of iron oxide that was still in

signal range). Although the T2 values gradually increased for samples B through E as the cell number decreased from $20x10^6$ (~700,000 cells/1 mm slice) to $5x10^6$ (~175,000 cells/1 mm slice) the T2 values were consistently low compared to the gelatin phantom that did not contain any iron-oxide, ranging between 15.4 ms and 48 ms. It is not until the cell number decreases to $1x10^6$ (~35,000 cells/1 mm slice) that the T2 value shows a significant increase to 140 ms. In other words, sample E is the first concentration of iron oxide where the signal void (T2 shortening) begins to become apparent compared to sample F and G (the control). Based on these T2 values the cellular limit of detection was determined to be between 175,000 and 35,000 cells. This detection limit fell well below the macrophage retention number after static seeding ($\sim 3.8 \times 10^5 \pm 13\%$ cells) providing evidence for the feasibility of MRI detection on our biodegradable scaffolds.

Next, to confirm the potential for cell tracking on a clinically relevant substrate, USPIO labeled macrophages were seeded onto biodegradable scaffolds for *in vitro* MRI analysis. Three scaffolds were suspended in Histogel® for MRI analysis and T2 mapping, one scaffold seeded with UPSIO labeled macrophages, one scaffold seeded with unlabeled macrophages, and one unseeded scaffold (Figure 2C, D). The T2 values for the scaffolds were 26.66 ms, 45.38 ms, and 84.50 ms, respectively (Table 3). The region of signal void created around the scaffold seeded with labeled macrophages was significantly larger than the void created by the scaffold seeded with unlabeled macrophages or the unseeded scaffold. This confirmed that labeling macrophages with USPIO substantially reduced the MRI signal intensity around the scaffold making it appear uniformly dark and easily detectable on MRI. In addition,

the USPIO labeled scaffold appeared larger than either of the other scaffolds secondary to the "blooming effect," an amplification of signal change on gradient-echo images where T2 effects dominate, which increases visibility on MRI. Interestingly the T2 value for the USPIO seeded scaffold was 26.66 ms, a number that closely resembles the T2 value calculated for the USPIO cell suspension containing ~350,000 cells/1 mm slice (22 ms, sample D). Given that the macrophage retention after static seeding is approximately 300,000 cells these numbers closely correspond and provide further evidence for the correlation of T2 values with cell number for cell tracking *in vivo*.

Through MR phantom imaging, the *in vitro* detection limit for USPIO-labeled macrophages was determined, and the potential for cell tracking on a clinically relevant substrate was demonstrated, providing the necessary background to begin noninvasive cell tracking on the TEVGs *in vivo* with MR imaging.

In vivo Serial MRI Analysis and Cell Tracking

For *in vivo* MRI analysis four SCID/beige mice were surgically implanted with TEVGs seeded with USPIO-labeled macrophages, and four SCID/beige mice serving as controls were implanted with TEVGs seeded with unlabeled macrophages. The TEVGs were implanted as infrarenal interposition grafts in the inferior vena cavas (IVCs) of the mice. After implantation, Rare T2 weighted images were obtained immediately postoperatively and at one week post-implantation in all the mice.

Representative Rare T2 weighted images and their corresponding T2 maps are shown in Figure 3.

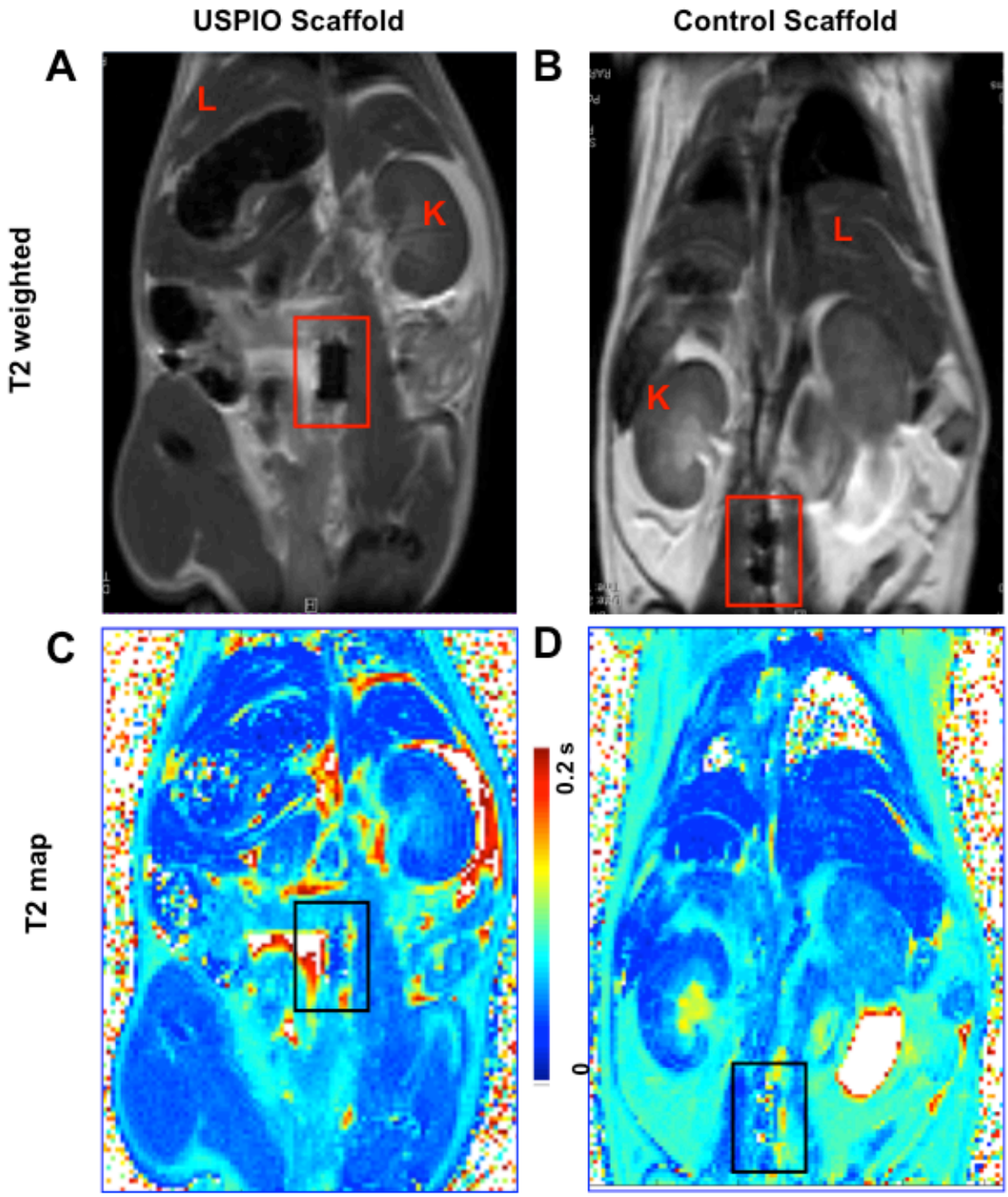

Figure 3*. In vivo* MR Imaging of Labeled and Unlabeled Scaffold Implants. Representative axial T2 weighted RARE images of mice implanted with (A) labeled and (B) unlabeled seeded scaffolds, illustrating the location of implanted scaffolds (boxes). Kidneys (K) and the liver (L) are visible in the images. The corresponding

T2 maps of the same slices showing T2 value differences between the (C) labeled and (D) unlabeled seeded scaffolds.

The TEVGs were easily identified retroperitoneally in the infrarenal IVCs of the mice, both immediately after implantation, and after 1 week. T2 values were calculated for the TEVGs seeded with both USPIO-labeled and unlabeled macrophages as well as for other tissues including the liver, muscle, and fat. The T2 values measured in all the tissues outside of the IVC implants were similar in both groups immediately after implantation and at one week postimplantation (Figure 4A, B).

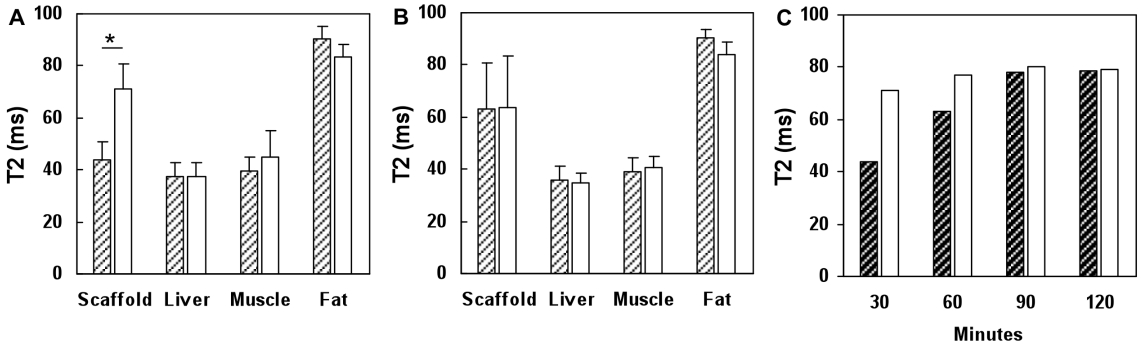

Figure 4. *In vivo* T2 Values for Serial MR Imaging of Scaffold Implants. T2 values for scaffold implants and extra-vascular tissues in mice with USPIO-labeled implants (dashed bars) and mice with non-USPIO-labeled implants (plain bars) imaged (A) immediately after implantation and (B) one week post implantation. To gain further insight into the temporal increase in the T2 value in the labeled scaffolds, T2 values were calculated for scaffold implants in one additional mouse with a USPIO-labeled implant (dark dashed bars) and one with a non-USPIO-labeled implant (plain bars) at 30-minute increments starting immediately after implantation (C).

The T2 maps reveal significantly lower T2 values in the TEVGs seeded with USPIO labeled macrophages immediately postoperatively (T2 = 44±6.8 vs. 71±10.2), (Figure 4A) that was no longer apparent at 7 days post-operatively (T2 = 63±12 vs. 63±14). The drop in the T2 values seen in the TEVGs seeded with USPIO-

macrophages verifies that the seeded macrophages were retained on the scaffold after surgical implantation in numbers greater than the MRI cellular limit of detection, and that large enough number of cells was lost from the scaffold by one week, such that the signal difference was no longer significantly detectable. In order to gain further insight into the time frame with which the USPIO seeded macrophages were lost from the scaffold implants additional mice were serially imaged in 30-minute increments immediately after scaffold implantation for up to 9 hours. The T2 values were calculated for each time point and showed a rapidly progressive increase in the T2 value for the USPIO-seeded scaffold (Figure 4C). The T2 value increased to control values by 90 minutes after implantation indicating that the cells are rapidly lost from the implanted TEVG.

Histological Analysis

These findings were verified with histology of USPIO-labeled and non-USPIO-labeled TEVG explants immediately after implantation (T=0), at two hours after implantation (after the T2 value is shown to increase to control levels), and one week after implantation. The scaffold explants were embedded in GMA and stained with Prussian blue to identify intracellular iron deposits. The number of cells containing intracellular iron deposits as well as the total number of cells in each scaffold was determined at each time point (Figure 5).

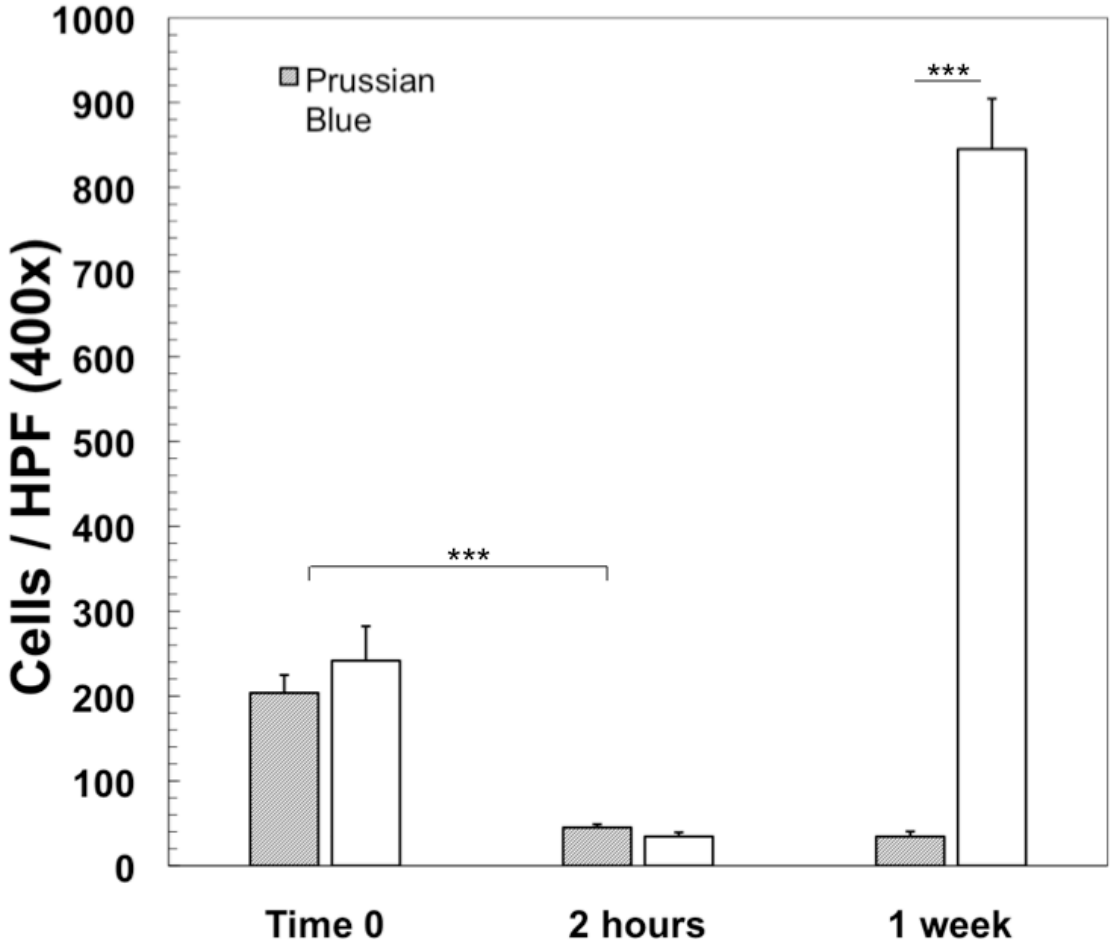

Figure 5. Fate of Seeded Cells by Histological Analysis. Scaffold explants were stained with Prussian blue to identify intracellular iron deposits. The number of Prussian blue labeled cells (dashed bars) and the total number of cells (plain bars) (per HPF) were counted immediately after implantation (Time=0), 2 hours, and one week after implantation.

There are significantly more Prussian blue stained USPIO labeled cells (203.625 ± 21.085 /HPF, 400x) visible immediately post-implantation (T=0) than after 2 hours (45.0 ± 3.830/HPF, 400x) or one week (34.333 ± 6.098/HPF, 400x). The number of Prussian blue stained cells is not significantly different after 2 hours or one week post-implantation, indicating that the majority of seeded cells are lost from the scaffold immediately after implantation in the animal. In addition, the total

number of cells in the scaffold at time 0 and after 2 hours is not significantly different from the number of Prussian blue labeled cells at these time points. However, by one week post-implantation the total number of cells in the scaffolds is significantly higher than the number of Prussian blue labeled cells due to host cell infiltration. These findings support the cellular MR imaging data correlating the rapid increase in T2 value post-implantation to the rapid loss of seeded cells from the TEVG.

Discussion

To our knowledge, this study is one of the first applications of noninvasive MR imaging to study the process of neotissue development in TEVGs through the use of serial imaging in a living animal model. We have used noninvasive serial MR imaging to support recently published data indicating that the bone marrow mononuclear cells used to seed the scaffolds pre-implantation are not incorporated into the neovessel as previously thought (17), but are instead rapidly lost from the TEVG post-implantation (33).

In order to accomplish this, we first optimized the macrophage USPIO incubation conditions in order to achieve adequate cell labeling, without affecting cellular viability or metabolic activity, providing a reasonable cellular limit of detection on our scaffolds both *in vitro* and *in vivo* by MRI. This was accomplished using USPIO nanoparticles without poly-l-lysine on their surface. Poly-l-lysine has traditionally been used in the field of cellular MRI to enhance the uptake of the MR contrast agents into various cell types by changing the surface charge of the particles. This, however, comes at the cost of increasing cellular toxicity of the nanoparticles (55). We found that while the use of poly-l-lysine shortened the incubation duration required to achieve 100% labeling efficiency, it had the adverse affect of impairing cellular metabolic activity and viability as determined by the MTS assay and 7-AAD flow cytometry when compared to unlabeled cells (data not shown). In the cell population composed entirely of macrophages and monocytes, which are traditionally known to robustly engulf MR contrast agents without the added help of poly-l-lysine (58,80), it was determined that adequate cell labeling

could be achieved without poly-l-lysine. We found that incubating the macrophages with a USPIO concentration of 2 mg/ml for 36 hours in serum free media resulted in 100% labeling efficiency without affecting cellular metabolic activity or viability. This is consistent with previous investigations in macrophage and monocyte cell lines that have found no significant toxic effects with a labeling concentration as high as 10mg/ml of USPIO (80).

Using these labeling conditions we were able to perform a limit of detection study to correlate USPIO labeled macrophage concentration with MR signal intensity. Serially diluted USPIO labeled cell suspensions were imaged and T2 mapping was performed. Since USPIO is a T2 contrast agent it creates a signal void or a hypodense change in signal intensity. As the concentration of USPIO labeled macrophages was incrementally increased the cell-suspension samples appeared increasingly darker with increasingly lower T2 values. Through an analysis of the quantitative T2 values we were able to correlate the USPIO labeled macrophage concentration with the T2 values and determined a limit of detection for our labeled cell population. This was based on the first detectable signal void or T2 shortening that occurred in one of our cell suspension samples compared to the control sample. The limit of detection was found to be between 175,000 and 35,000 cells. This is similar to the detection threshold of approximately 10^5 cells that is commonly cited in other literature looking at *in vivo* applications of USPIO cell tracking (44,83,84). This limit of detection threshold is dependent on several imaging parameters such as the spatial and temporal resolution and the magnetic field strength. Additionally, when the studies are being performed *in vivo,* there is the added complication of

motion artifact that occurs with the respiratory rate and the heart rate. Under ideal conditions and in organs where motion can almost be completely eliminated, such as in the brain, single cell detection has become possible (44,85-87). However, the field is still working towards this becoming a routine capability for use with *in vivo* models of cellular MRI. For our model of vascular tissue engineering and TEVG development, the detection limit is exactly what would be expected for an *in vivo* application dealing with an active circulating system and respiration.

It was also important to image grafts seeded with USPIO labeled macrophages to determine the potential for cell tracking on a clinically relevant substrate, and to allow cell concentration on the graft to be correlated with MR signal intensity. With a seeding efficiency of approximately 8%, we were able to effectively seed our biodegradable TEVG scaffolds with sufficient numbers of USPIO labeled macrophages to allow for *in vitro* quantification by MR imaging and T2 mapping. The scaffold seeded with USPIO-labeled macrophages appeared larger and darker than the scaffold seeded with unlabeled macrophages and had a remarkable decrease in T2 relaxivity due to the presence of iron oxide. The reason the USPIO labeled scaffold appeared larger than the unlabeled scaffold is due to the large magnetic susceptibility of iron oxide particles. This susceptibility can affect an area much larger than the actual size of the particles, leading to an exaggeration of the region occupied by iron oxide. This is referred to as the ”blooming effect,” an amplification of signal changes produced by microscopic inhomogeneities in the magnetic field that produce a rapid dephasing of diffusing water protons including those some distance away leading to a hypointense effect that extends beyond the

individual particles (42,47). This is a commonly cited disadvantage to the use of iron oxide for cellular MRI. However, in our current application the blooming effect has actually been beneficial in allowing for an increased sensitivity of detection of TEVGs within the native vessel background.

For the *in vivo* application, USPIO labeled biodegradable scaffolds were implanted as infrarenal interposition grafts in the inferior vena cavas of SCID/bg mice. T2 mapping of the IVC scaffold implants showed a drop in T2 signal intensity immediately after implantation that was no longer observed at either 2 hours or 1 week post-implantation. In order to get a better temporal picture of the frequency with which the USPIO-labeled cells were lost from the implanted scaffold, we performed serial images on a mouse with a USPIO-labeled implant every 30 minutes, until the T2 signal had increased to values seen in control mice with unlabeled implants. The T2 signal increased to control levels within 90 minutes of implantation. This rapid increase in T2 signal intensity correlates with the loss of USPIO labeled cells from the scaffolds. To verify our findings, TEVGs were explanted and stained with Prussian blue for the presence of iron oxide labeled cells. The number of iron oxide labeled cells decreases significantly as early as two hours post-implantation. The number of iron oxide labeled cells is not statistically different from two hours to one week post-implantation, leading us to believe that all of the iron oxide labeled cells are lost from the implanted scaffold immediately after implantation. This corresponds very nicely with the rapid rise in the T2 value at 2 hours post-implantation.

This data supports the recently published data by Roh *et al.* (33) showing that by one week post-implantation, there are no longer any seeded human BMCs detectable in the neovessel. Roh *et al.* concluded that, in contrast to prior studies reporting that the seeded BMCs gave rise to the cells of the neovessel, the seeded cells are rapidly lost from the implanted TEVG. Here, we have verified this same data by utilizing cellular MRI to track the fate of the seeded cells in our small animal model of TEVG development. This data is consistent with the new inflammatory-mediated model of vascular remodeling. This model hypothesizes that the process of neovessel formation is not driven by stem cells within the seeded BMC population differentiating into mature cells of the neovessel, but that instead the seeded BMCs are responsible for secreting a host of inflammatory mediators that recruit host inflammatory cells to the TEVG that initiates an inflammation driven process of neovessel formation. Not only do these findings provide additional evidence for this novel school of thought about the mechanism of neotissue development in TEVGs, but these answers to critical questions regarding neovessel formation were obtained by utilizing cellular MRI, a noninvasive *in vivo* technique.

One major limitation in the field of tissue engineering is the lack of advanced analytical tools, especially those that allow noninvasive monitoring of tissue development. Currently, the most widely used method for characterizing tissue engineered constructs consists of sacrificing the animal host, harvesting the construct, and performing histology. This approach results in the destruction of the sample and precludes longitudinal studies with the same tissue engineered samples (51). To overcome this problem, many groups have begun to focus on incorporating

noninvasive cellular MR imaging techniques to study their tissue-engineering applications. Although the use of molecular and cellular MRI is still very limited in the field of tissue engineering, it is increasingly being realized that the future of the field will greatly benefit from this noninvasive approach to studying dynamic changes that occur during neotissue development *in vivo*. The paucity of noninvasive techniques currently available to monitor the fate of transplanted tissue engineered constructs is commonly cited as one of the major challenges facing the translation of regenerative medicine into the clinical realm (74).

The field of cellular MRI is a burgeoning field that allows noninvasive monitoring of biological processes *in vivo* (68). In has been widely used for cell tracking and enhanced visualization of *in vivo* processes, with related areas of research also using MRI contrast agent cell labeling to guide cell delivery and to enhance cellular therapeutic approaches with interventional MRI (44,88,89). A noninvasive approach is instrumental for determining the trafficking and biodistribution of cells *in vivo* after delivery, whether they are functioning or have differentiated into the desired cell type, and whether the cells reach their target and how long they reside there. All of the information gained from tracking can be used to ensure the appropriate route of delivery, provide feedback into the preferred site of engraftment and aid in determining the optimal dosing schedule and numbers of cells to be used to achieve desired therapeutic outcome (90).

For cell tracking purposes, the most widely used applications consist of cellular tracking of macrophages in CNS and atherosclerotic disease (58-61) providing evidence that it would be well suited for a similar purpose in vascular

tissue engineering. However, to date, most applications of cellular MRI in the field of vascular tissue engineering have been limited to mostly proof-of-principle studies that show the promising feasibility of using these technologies in the future to study TEVG development and in the clinical setting to monitor graft patency (79,42,75). To our knowledge, no group has used cellular MRI technology to answer a question about the mechanism of *in vivo* neovessel development in vascular tissue engineering prior to this study. We are setting the stage for the future of noninvasive monitoring studies to help delineate the exact mechanism of neovessel development with the hopes of creating improved TEVGs for use in congenital heart surgery. In addition, a noninvasive monitoring technique in the clinical setting would allow physicians to monitor the development and function of TEVGs in patients with the idea that visualization of aberrant development could potentially lead to early therapeutic intervention.

This data is very promising for the use of cellular MRI in vascular tissue engineering. However, there are still several limitations associated with the use of USPIO particles for cell tracking and with the currently available MRI technology. While the use of iron oxide based contrast agents is currently the predominantly utilized nanoparticle contrast agent for cellular MRI there are still several limitations surrounding their use. One major limitation is the fact that iron oxide is a T2 contrast agent that creates a negative contrast or hypointense (dark) signal. This signal may be confounded with similar hypointense MR signals originating from the vasculature, hemorrhages, or tumors (54). In addition, void detection is dependent on image resolution which is limited by partial volume effects (90).

These drawbacks are being overcome by the trend of producing agents with lower thresholds of detectability, the installation of scanners with higher field strengths (55), and a focus on imaging the off-resonance effects (44). A final solution to this problem involves the development of Gadolinium based nanoparticulate contrast agents that have better cell toxicity profiles (91).

Another confounding factor is the possibility that the loss of MR signal could be caused by dilution of the contrast agent through cell division or biodegradation instead of dispersion of cells carrying the label (79). There has been some initial work on overcoming this problem of signal dilution secondary to cell division by utilizing MR reporter genes or contrast agents that are activated by conditional upregulation of enzymes (92,93). However, many research groups have shown that although the iron load is diluted with cell division, the signal is still strong enough to be detected for at least seven days and even longer depending on the rate of cell division and initial iron load (57,74,79).

In our work, it is possible that the increase in T2 signal was caused by the rapid exocytosis or metabolism of the iron oxide particles. However, this is unlikely due to the time frame with which the signal increased and previously reported evidence that macrophages are able to retain endocytosed iron oxide particles in large enough quantities produce a drop in MR signal intensity for at least ten days post-labeling (80). Terrovitis *et al.* (75) demonstrated ferumoxide labeling that remained effective on scans up to four weeks after the labeling procedure.

One major limitation with bringing this technology into the clinical realm is the current lack of interest in MR-compatible device development (44). MRI has not

yet become a part of standard laboratory equipment. This is mostly due to the large investment that goes into maintaining a superconducting MRI device as well as the lack of development of specially designed coils and other equipment necessary to image samples of multiple sizes and shapes (51). In addition, the most widely used strategy for increasing the spatial resolution (a requirement for cell tracking application) requires the use of high-field MRI to increase the signal to noise ratio (SNR) in a voxel by enhancing the magnetic field strength. However, high-field MRI is not currently available in the clinical setting and has several limitations such as high cost, reduced bore size, and artifact susceptibility. Poirier-Quinot *et al.* propose an alternative approach using a high-temperature superconducting (HTS) cryo-cooled detection coil to increase the SNR (74). Yet, this approach also has a major limitation in that it only permits high-resolution in a small volume limiting the region of interest that can be visualized.

Another alternative approach was recently published by Nitzsche *et al.,* demonstrating the feasibility of using benchtop-MRI (BT-MRI) as an affordable and powerful analytic tool for monitoring tissue engineered constructs (51). The main reason that BT-MRI is more affordable is due to the low static magnetic field strength of 0.5T and the absence of a helium cooling system. Nitzsche *et al.* demonstrated the ability of BT-MRI to characterize tissue-engineered scaffolds as well as to track SPIO-labeled cells seeded onto the scaffolds. They concluded that this might open the door for BT-MRI to become a more lab-oriented and accessible tool for monitoring tissue-engineered constructs allowing for the advancement of MRI as a tool for noninvasive monitoring in tissue engineering applications.

Although there are still significant limitations with this technology, more groups are realizing the importance of using noninvasive techniques to study the dynamic changes that occur as their tissue-engineered constructs develop. Noninvasive monitoring of tissue growth is required for the future of tissue engineering and these techniques are becoming a focus in the field. In our research group, we are already beginning to build on our current results by performing additional cell tracking studies that will help refine our knowledge of how neotissue develops in our model of TEVG development. We have been able to show the rapid loss of seeded cells from the implanted TEVG and now we are working to show the infiltration of cells into the TEVG from the host. From previous reports we know that after the seeded cells are lost from the implanted TEVG, there is a rapid infiltration of host macrophages that initiate an inflammatory process of vascular remodeling (33). The next phase of this research will involve labeling host macrophages with USPIO and tracking their infiltration into implanted TEVGs with cellular MRI. To accomplish this we will try both *ex vivo* and *in vivo* macrophage cell labeling. In the former method, macrophages will be incubated with USPIO particles *ex vivo* and then injected into SCID/bg mice after they have had TEVGs implanted. In the latter method, USPIO particles will be injected into SCID/bg mice to see if adequate *in vivo* macrophage cell labeling can be achieved. In both cases, serial MR imaging will be performed to follow the migration of USPIO-labeled macrophages into the TEVG from the host vasculature.

Once this technology becomes more widespread with the development of more sensitive MR contrast agents and with increased access to more advanced MR

technology it is easy to see how it will become an integral part of vascular tissue engineering. The future of cellular MRI goes beyond noninvasive monitoring and can extend into the realm of directed TEVG development by coupling MRI contrast agents with drug delivery systems (54). In clinical applications, noninvasive monitoring of macrophages can be used as an early method to identify patients at risk for graft stenosis leading to early intervention. Cellular MRI is a powerful tool in the field of vascular tissue engineering that is critical to delineating the specific mechanism of neovessel development as TEVGs undergo dynamic changes in our small animal model. Knowledge gained through this research will be instrumental in creating improved TEVGs, for directing neovessel development, and for use in the clinical setting as a valuable monitoring technique to improve patient outcomes.

References

1. American Heart Association [Internet]. [cited 2011 Jan 29];Available from: http://www.heart.org/HEARTORG/

2. Welcome to the Pediatric Heart Network (PHN) [Internet]. [cited 2011 Jan 29];Available from: http://www.pediatricheartnetwork.org/whatisphnforpractitioners.asp

3. Hibino N, McGillicuddy E, Matsumura G, Ichihara Y, Naito Y, Breuer C, et al. Late-term results of tissue-engineered vascular grafts in humans. The Journal of Thoracic and Cardiovascular Surgery. 2010 Feb;139(2):431-436.e2.

4. Hoffman JIE, Kaplan S. The incidence of congenital heart disease. J. Am. Coll. Cardiol. 2002 Jun 19;39(12):1890-1900.

5. Zannini L, Borini I. State of the art of cardiac surgery in patients with congenital heart disease. J Cardiovasc Med (Hagerstown). 2007 Jan;8(1):3-6.

6. Kim S, Kim W, Lim H, Lee J. Outcome of 200 patients after an extracardiac Fontan procedure. The Journal of Thoracic and Cardiovascular Surgery. 2008 Jul;136(1):108-116.

7. Fontan F, Baudet E. Surgical repair of tricuspid atresia. Thorax. 1971 May 1;26::240 -248.

8. Alexi-Meskishvili V, Ovroutski S, Ewert P, Dähnert I, Berger F, Lange PE, et al. Optimal conduit size for extracardiac Fontan operation. European Journal of Cardio-Thoracic Surgery. 2000 Dec;18(6):690-695.

9. Giannico S, Hammad F, Amodeo A, Michielon G, Drago F, Turchetta A, et al. Clinical Outcome of 193 Extracardiac Fontan Patients: The First 15 Years. Journal of the American College of Cardiology. 2006 May 16;47(10):2065-2073.

10. Gentles TL, Gauvreau K, Mayer JE, Fishberger SB, Burnett J, Colan SD, et al. FUNCTIONAL OUTCOME AFTER THE FONTAN OPERATION: FACTORS INFLUENCING LATE MORBIDITY. J Thorac Cardiovasc Surg. 1997 Sep 1;114(3):392-403.

11. Mirensky TL, Breuer CK. The development of tissue-engineered grafts for reconstructive cardiothoracic surgical applications. Pediatr. Res. 2008 May;63(5):559-568.

12. Langer R, Vacanti J. Tissue engineering. Science. 1993 May 14;260(5110):920 -926.

13. Sodian R, Fu P, Lueders C, Szymanski D, Fritsche C, Gutberlet M, et al. Tissue Engineering of Vascular Conduits: Fabrication of Custom-Made Scaffolds Using Rapid Prototyping Techniques. Thorac cardiovasc Surg. 2005 6;53(3):144-149.

14. Matsumura G, Hibino N, Ikada Y, Kurosawa H, Shin'oka T. Successful application of tissue engineered vascular autografts: clinical experience. Biomaterials. 2003 Jun;24(13):2303-2308.

15. Brennan MP, Dardik A, Hibino N, Roh JD, Nelson GN, Papademitris X, et al. Tissue-engineered Vascular Grafts Demonstrate Evidence of Growth and Development When Implanted in a Juvenile Animal Model. Transactions of the ... Meeting of the American Surgical Association. 2008;126:20-27.

16. Shinoka T, Shum-Tim D, Ma PX, Tanel RE, Isogai N, Langer R, et al. Creation of viable pulmonary artery autografts through tissue engineering. J. Thorac. Cardiovasc. Surg. 1998 Mar;115(3):536-545; discussion 545-546.

17. Matsumura G, Miyagawa-Tomita S, Shin'oka T, Ikada Y, Kurosawa H. First Evidence That Bone Marrow Cells Contribute to the Construction of Tissue-Engineered Vascular Autografts *In vivo*. Circulation. 2003 Oct 7;108(14):1729-1734.

18. Shinoka T, Breuer C. Tissue-Engineered Blood Vessels in Pediatric Cardiac Surgery. Yale J Biol Med. 2008 Dec;81(4):161-166.

19. Roh JD, Nelson GN, Brennan MP, Mirensky TL, Yi T, Hazlett TF, et al. Small-diameter biodegradable scaffolds for functional vascular tissue engineering in the mouse model. Biomaterials. 2008 Apr;29(10):1454-1463.

20. Shin'oka T, Imai Y, Ikada Y. Transplantation of a tissue-engineered pulmonary artery. N. Engl. J. Med. 2001 Feb 15;344(7):532-533.

21. Naito Y, Imai Y, Shinoka T, Kashiwagi J, Aoki M, Watanabe M, et al. Successful clinical application of tissue-engineered graft for extracardiac Fontan operation. Journal of Thoracic and Cardiovascular Surgery. 2003 2;125(2):419-420.

22. Isomatsu Y, Shin'oka T, Matsumura G, Hibino N, Konuma T, Nagatsu M, et al. Extracardiac total cavopulmonary connection using a tissue-engineered graft. Journal of Thoracic and Cardiovascular Surgery. 2003 Dec;126(6):1958-1962.

23. Shin'oka T, Matsumura G, Hibino N, Naito Y, Watanabe M, Konuma T, et al. Midterm clinical result of tissue-engineered vascular autografts seeded with autologous bone marrow cells. The Journal of Thoracic and Cardiovascular Surgery. 2005 Jun;129(6):1330-1338.

24. Nelson GN, Mirensky T, Brennan MP, Roh JD, Yi T, Wang Y, et al. Functional

Small-Diameter Human Tissue-Engineered Arterial Grafts in an Immunodeficient Mouse Model: Preliminary Findings. Arch Surg. 2008 May 1;143(5):488-494.

25. Lopez-Soler RI, Brennan MP, Goyal A, Wang Y, Fong P, Tellides G, et al. Development of a mouse model for evaluation of small diameter vascular grafts. J. Surg. Res. 2007 May 1;139(1):1-6.

26. Noishiki Y, Tomizawa Y, Yamane Y, Matsumoto A. Autocrine angiogenic vascular prosthesis with bone marrow transplantation. Nat Med. 1996 Jan;2(1):90-93.

27. Shi Q, Rafii S, Wu MH, Wijelath ES, Yu C, Ishida A, et al. Evidence for Circulating Bone Marrow-Derived Endothelial Cells. Blood. 1998 Jul 15;92(2):362-367.

28. Hristov M, Erl W, Weber PC. Endothelial progenitor cells: mobilization, differentiation, and homing. Arterioscler. Thromb. Vasc. Biol. 2003 Jul 1;23(7):1185-1189.

29. Asahara T, Masuda H, Takahashi T, Kalka C, Pastore C, Silver M, et al. Bone marrow origin of endothelial progenitor cells responsible for postnatal vasculogenesis in physiological and pathological neovascularization. Circ. Res. 1999 Aug 6;85(3):221-228.

30. Kaushal S, Amiel GE, Guleserian KJ, Shapira OM, Perry T, Sutherland FW, et al. Functional small-diameter neovessels created using endothelial progenitor cells expanded *ex vivo*. Nat. Med. 2001 Sep;7(9):1035-1040.

31. Assmus B, Schächinger V, Teupe C, Britten M, Lehmann R, Döbert N, et al. Transplantation of Progenitor Cells and Regeneration Enhancement in Acute Myocardial Infarction (TOPCARE-AMI). Circulation. 2002 Dec 10;106(24):3009-3017.

32. Tateishi-Yuyama E, Matsubara H, Murohara T, Ikeda U, Shintani S, Masaki H, et al. Therapeutic angiogenesis for patients with limb ischaemia by autologous transplantation of bone-marrow cells: a pilot study and a randomised controlled trial. Lancet. 2002 Aug 10;360(9331):427-435.

33. Roh JD, Sawh-Martinez R, Brennan MP, Jay SM, Devine L, Rao DA, et al. Tissue-engineered vascular grafts transform into mature blood vessels via an inflammation-mediated process of vascular remodeling. Proceedings of the National Academy of Sciences. 2010 Mar 9;107(10):4669 -4674.

34. Zentilin L, Tafuro S, Zacchigna S, Arsic N, Pattarini L, Sinigaglia M, et al. Bone marrow mononuclear cells are recruited to the sites of VEGF-induced neovascularization but are not incorporated into the newly formed vessels. Blood. 2006 May 1;107(9):3546-3554.

35. Ziegelhoeffer T, Fernandez B, Kostin S, Heil M, Voswinckel R, Helisch A, et al. Bone Marrow-Derived Cells Do Not Incorporate Into the Adult Growing Vasculature. Circ Res. 2004 Feb 6;94(2):230-238.

36. Yamanami M, Yamamoto A, Iida H, Watanabe T, Kanda K, Yaku H, et al. 3-Tesla magnetic resonance angiographic assessment of a tissue-engineered small-caliber vascular graft implanted in a rat. J. Biomed. Mater. Res. 2010 1;92B(1):156-160.

37. Xu H, Othman SF, Magin RL. Monitoring Tissue Engineering Using Magnetic Resonance Imaging. Journal of Bioscience and Bioengineering. 2008 Dec;106(6):515-527.

38. Burtea C, Laurent S, Mahieu I, Larbanoix L, Roch A, Port M, et al. *In vitro* biomedical applications of functionalized iron oxide nanoparticles, including those not related to magnetic properties. Contrast Media Mol Imaging. 2010;:n/a-n/a.

39. Burtea C, Laurent S, Vander Elst L, Muller RN. Contrast agents: magnetic resonance. Handb Exp Pharmacol. 2008;(185 Pt 1):135-165.

40. Rogers WJ, Meyer CH, Kramer CM. Technology insight: *in vivo* cell tracking by use of MRI. Nat Clin Pract Cardiovasc Med. 2006 Oct;3(10):554-562.

41. Shapiro EM, Medford-Davis LN, Fahmy TM, Dunbar CE, Koretsky AP. Antibody-mediated cell labeling of peripheral T cells with micron-sized iron oxide particles (MPIOs) allows single cell detection by MRI. Contrast Media Mol Imaging. 2007 5;2(3):147-153.

42. Bulte JWM, Duncan ID, Frank JA. *In vivo* Magnetic Resonance Tracking of Magnetically Labeled Cells After Transplantation. J Cereb Blood Flow Metab. 2002;22(8):899-907.

43. Wilhelm C, Bal L, Smirnov P, Galy-Fauroux I, Clément O, Gazeau F, et al. Magnetic control of vascular network formation with magnetically labeled endothelial progenitor cells. Biomaterials. 2007 Sep;28(26):3797-3806.

44. Kraitchman DL, Gilson WD, Lorenz CH. Stem cell therapy: MRI guidance and monitoring. J Magn Reson Imaging. 2008 Feb;27(2):299-310.

45. de Vries IJM, Lesterhuis WJ, Barentsz JO, Verdijk P, van Krieken JH, Boerman OC, et al. Magnetic resonance tracking of dendritic cells in melanoma patients for monitoring of cellular therapy. Nat. Biotechnol. 2005 Nov;23(11):1407-1413.

46. Crich SG, Biancone L, Cantaluppi V, Du D, Esposito G, Russo S, et al. Improved route for the visualization of stem cells labeled with a Gd-/Eu-Chelate as dual (MRI and fluorescence) agent. Magn. Reson. Med. 2004 5;51(5):938-944.

47. Rogers WJ, Meyer CH, Kramer CM. Technology Insight: *in vivo* cell tracking by use of MRI. Nat Clin Pract Cardiovasc Med. 2006 10;3(10):554-562.

48. Helmchen F, Denk W. Deep tissue two-photon microscopy. Nat. Methods. 2005 Dec;2(12):932-940.

49. Miller MJ, Wei SH, Cahalan MD, Parker I. Autonomous T cell trafficking examined *in vivo* with intravital two-photon microscopy. Proc. Natl. Acad. Sci. U.S.A. 2003 Mar 4;100(5):2604-2609.

50. Wei SH, Miller MJ, Cahalan MD, Parker I. Two-photon imaging in intact lymphoid tissue. Adv. Exp. Med. Biol. 2002;512:203-208.

51. Nitzsche H, Metz H, Lochmann A, Bernstein A, Hause G, Groth T, et al. Characterization of Scaffolds for Tissue Engineering by Benchtop-Magnetic Resonance Imaging. Tissue Engineering Part C: Methods. 2009 9;15(3):513-521.

52. Bulte JW. Intracellular endosomal magnetic labeling of cells. In: Magnetic Resonance Imaging: Methods and Biological Applications. Humana Press, Springer, Berlin, Germany; 2006. p. 419-439.

53. Crich SG, Biancone L, Cantaluppi V, Duò D, Esposito G, Russo S, et al. Improved route for the visualization of stem cells labeled with a Gd-/Eu-chelate as dual (MRI and fluorescence) agent. Magn Reson Med. 2004 May;51(5):938-944.

54. Kubinová Š, Syková E. Nanotechnologies in regenerative medicine. Minim Invasive Ther Allied Technol. 2010 6;19(3):144-156.

55. Bulte JWM, Kraitchman DL. Iron oxide MR contrast agents for molecular and cellular imaging. NMR Biomed. 2004 Nov;17(7):484-499.

56. Heyn C, Bowen CV, Rutt BK, Foster PJ. Detection threshold of single SPIO-labeled cells with FIESTA. Magn Reson Med. 2005 Feb;53(2):312-320.

57. Strijkers GJ, Mulder WJM, van Tilborg GAF, Nicolay K. MRI contrast agents: current status and future perspectives. Anticancer Agents Med Chem. 2007 May;7(3):291-305.

58. Trivedi RA, U-King-Im J, Graves MJ, Cross JJ, Horsley J, Goddard MJ, et al. *In vivo* detection of macrophages in human carotid atheroma: temporal dependence of ultrasmall superparamagnetic particles of iron oxide-enhanced MRI. Stroke. 2004 Jul;35(7):1631-1635.

59. Corot C, Petry KG, Trivedi R, Saleh A, Jonkmanns C, Le Bas J, et al. Macrophage imaging in central nervous system and in carotid atherosclerotic plaque using ultrasmall superparamagnetic iron oxide in magnetic resonance imaging. Invest

Radiol. 2004 Oct;39(10):619-625.

60. Kooi ME, Cappendijk VC, Cleutjens KBJM, Kessels AGH, Kitslaar PJEHM, Borgers M, et al. Accumulation of ultrasmall superparamagnetic particles of iron oxide in human atherosclerotic plaques can be detected by *in vivo* magnetic resonance imaging. Circulation. 2003 May 20;107(19):2453-2458.

61. Ruehm SG, Corot C, Vogt P, Kolb S, Debatin JF. Magnetic resonance imaging of atherosclerotic plaque with ultrasmall superparamagnetic particles of iron oxide in hyperlipidemic rabbits. Circulation. 2001 Jan 23;103(3):415-422.

62. Stoll G, Bendszus M. Imaging of inflammation in the peripheral and central nervous system by magnetic resonance imaging. Neuroscience. 2009 Feb 6;158(3):1151-1160.

63. Islam T, Josephson L. Current state and future applications of active targeting in malignancies using superparamagnetic iron oxide nanoparticles. Cancer Biomark. 2009;5(2):99-107.

64. Yang J, Liu J, Niu G, Chan KC, Wang R, Liu Y, et al. *In vivo* MRI of endogenous stem/progenitor cell migration from subventricular zone in normal and injured developing brains. Neuroimage. 2009 Nov 1;48(2):319-328.

65. Medarova Z, Vallabhajosyula P, Tena A, Evgenov N, Pantazopoulos P, Tchipashvili V, et al. *In vivo* imaging of autologous islet grafts in the liver and under the kidney capsule in non-human primates. Transplantation. 2009 Jun 15;87(11):1659-1666.

66. Politi LS, Bacigaluppi M, Brambilla E, Cadioli M, Falini A, Comi G, et al. Magnetic-resonance-based tracking and quantification of intravenously injected neural stem cell accumulation in the brains of mice with experimental multiple sclerosis. Stem Cells. 2007 Oct;25(10):2583-2592.

67. He G, Zhang H, Wei H, Wang Y, Zhang X, Tang Y, et al. *In vivo* imaging of bone marrow mesenchymal stem cells transplanted into myocardium using magnetic resonance imaging: a novel method to trace the transplanted cells. Int. J. Cardiol. 2007 Jan 2;114(1):4-10.

68. Towner RA, Smith N, Asano Y, He T, Doblas S, Saunders D, et al. Molecular magnetic resonance imaging approaches used to aid in the understanding of angiogenesis *in vivo*: implications for tissue engineering. Tissue Eng Part A. 2010 Feb;16(2):357-364.

69. Perea H, Aigner J, Heverhagen JT, Hopfner U, Wintermantel E. Vascular tissue engineering with magnetic nanoparticles: seeing deeper. J Tissue Eng Regen Med. 2007 Aug;1(4):318-321.

70. Shimizu K, Ito A, Arinobe M, Murase Y, Iwata Y, Narita Y, et al. Effective cell-seeding technique using magnetite nanoparticles and magnetic force onto decellularized blood vessels for vascular tissue engineering. J. Biosci. Bioeng. 2007 May;103(5):472-478.

71. Ito A, Ino K, Hayashida M, Kobayashi T, Matsunuma H, Kagami H, et al. Novel methodology for fabrication of tissue-engineered tubular constructs using magnetite nanoparticles and magnetic force. Tissue Eng. 2005 Oct;11(9-10):1553-1561.

72. Villalona GA, Udelsman B, Duncan DR, McGillicuddy E, Sawh-Martinez RF, Hibino N, et al. Cell-seeding techniques in vascular tissue engineering. Tissue Eng Part B Rev. 2010 Jun;16(3):341-350.

73. Wilhelm C, Bal L, Smirnov P, Galy-Fauroux I, Clément O, Gazeau F, et al. Magnetic control of vascular network formation with magnetically labeled endothelial progenitor cells. Biomaterials. 2007 Sep;28(26):3797-3806.

74. Poirier-Quinot M, Frasca G, Wilhelm C, Luciani N, Ginefri J, Darrasse L, et al. High-Resolution 1.5-Tesla Magnetic Resonance Imaging for Tissue-Engineered Constructs: A Noninvasive Tool to Assess Three-Dimensional Scaffold Architecture and Cell Seeding. Tissue Engineering Part C: Methods. 2010 4;16(2):185-200.

75. Terrovitis JV, Bulte JW, Sarvananthan S, Crowe LA, Sarathchandra P, Batten P, et al. Magnetic Resonance Imaging of Ferumoxide-Labeled Mesenchymal Stem Cells Seeded on Collagen Scaffolds?Relevance to Tissue Engineering. Tissue Engineering. 2006 10;12(10):2765-2775.

76. Heymer A, Haddad D, Weber M, Gbureck U, Jakob PM, Eulert J, et al. Iron oxide labelling of human mesenchymal stem cells in collagen hydrogels for articular cartilage repair. Biomaterials. 2008 Apr;29(10):1473-1483.

77. Saldanha KJ, Piper SL, Ainslie KM, Kim HT, Majumdar S. Magnetic resonance imaging of iron oxide labelled stem cells: applications to tissue engineering based regeneration of the intervertebral disc. Eur Cell Mater. 2008;16:17-25.

78. Ko IK, Song H, Cho E, Lee ES, Huh Y, Suh J. *In vivo* MR imaging of tissue-engineered human mesenchymal stem cells transplanted to mouse: a preliminary study. Ann Biomed Eng. 2007 Jan;35(1):101-108.

79. Nelson GN, Roh JD, Mirensky TL, Wang Y, Yi T, Tellides G, et al. Initial evaluation of the use of USPIO cell labeling and noninvasive MR monitoring of human tissue-engineered vascular grafts *in vivo*. FASEB J. 2008 Nov 1;22(11):3888-3895.

80. Müller K, Skepper JN, Posfai M, Trivedi R, Howarth S, Corot C, et al. Effect of ultrasmall superparamagnetic iron oxide nanoparticles (Ferumoxtran-10) on human monocyte-macrophages *in vitro*. Biomaterials. 2007 Mar;28(9):1629-1642.

81. Metz S, Bonaterra G, Rudelius M, Settles M, Rummeny EJ, Daldrup-Link HE. Capacity of human monocytes to phagocytose approved iron oxide MR contrast agents *in vitro*. Eur Radiol. 2004 Oct;14(10):1851-1858.

82. Anzai Y, Prince MR. Iron oxide-enhanced MR lymphography: the evaluation of cervical lymph node metastases in head and neck cancer. J Magn Reson Imaging. 1997 Feb;7(1):75-81.

83. Arbab AS, Frank JA. Cellular MRI and its role in stem cell therapy. Regen Med. 2008 Mar;3(2):199-215.

84. Feigenbaum GS, Lemberg L, Hare JM. Tracking cell fate with noninvasive imaging. J. Am. Coll. Cardiol. 2009 Oct 20;54(17):1627-1628.

85. Bulte JWM, Kraitchman DL. Monitoring cell therapy using iron oxide MR contrast agents. Curr Pharm Biotechnol. 2004 Dec;5(6):567-584.

86. Liu W, Frank JA. Detection and Quantification of Magnetically Labeled Cells by Cellular MRI. Eur J Radiol. 2009 May;70(2):258-264.

87. Mohs AM, Lu Z. Gadolinium(III)-based blood-pool contrast agents for magnetic resonance imaging: status and clinical potential. Expert Opin. Drug Deliv. 2007 3;4(2):149-164.

88. Gilad AA, Winnard PT, van Zijl PCM, Bulte JWM. Developing MR reporter genes: promises and pitfalls. NMR Biomed. 2007 May;20(3):275-290.

89. Hoehn M, Himmelreich U, Kruttwig K, Wiedermann D. Molecular and cellular MR imaging: potentials and challenges for neurological applications. J Magn Reson Imaging. 2008 May;27(5):941-954.

90. Hill JM, Dick AJ, Raman VK, Thompson RB, Yu Z, Hinds KA, et al. Serial cardiac magnetic resonance imaging of injected mesenchymal stem cells. Circulation. 2003 Aug 26;108(8):1009-1014.

91. Fahmy TM, Fong PM, Park J, Constable T, Saltzman WM. Nanosystems for simultaneous imaging and drug delivery to T cells. AAPS J. 2007 6;9(2):E171-E180.